frontiers in Environmental Science

TYPE Original Research
PUBLISHED 10 June 2026
DOI 10.3389/fenvs.2026.1805563

Check for updates

OPEN ACCESS

EDITED BY
Susan Page,
University of Leicester, United Kingdom

REVIEWED BY
Maciej Bartold,
Institute of Geodesy and Cartography, Poland
Oleksandr Melnyk,
Lesya Ukrainka Volyn National University, Ukraine

*CORRESPONDENCE
Christina Hellmann,
christina.hellmann@uni-greifswald.de

RECEIVED 06 February 2026
REVISED 17 April 2026
ACCEPTED 21 April 2026
PUBLISHED 10 June 2026

CITATION
Hellmann C, Watzig C, Pham V-D, Schwieder M and van der Linden S (2026) Mapping peatland species fractions and condition using multi-temporal spaceborne imaging spectroscopy data. *Front. Environ. Sci.* 14:1805563. doi: 10.3389/fenvs.2026.1805563

COPYRIGHT
© 2026 Hellmann, Watzig, Pham, Schwieder and van der Linden. This is an open-access article distributed under the terms of the Creative Commons Attribution License (CC BY). The use, distribution or reproduction in other forums is permitted, provided the original author(s) and the copyright owner(s) are credited and that the original publication in this journal is cited, in accordance with accepted academic practice. No use, distribution or reproduction is permitted which does not comply with these terms.

Mapping peatland species fractions and condition using multi-temporal spaceborne imaging spectroscopy data

Christina Hellmann[1]*, Cody Watzig[1], Vu-Dong Pham[1,2], Marcel Schwieder[3] and Sebastian van der Linden[1,2]

[1]Institute of Geology and Geography, University of Greifswald, partner in the Greifswald Mire Centre, University of Greifswald, Greifswald, Germany, [2]Interdisciplinary Centre for Baltic Sea Region Research (IFZO), University of Greifswald, Greifswald, Germany, [3]Thünen-Institute, Institute of Farm Economics, Braunschweig, Germany

Rewetting drained peatlands is crucial in mitigating climate change, but special monitoring schemes are required to track rewetting effects. Species distribution and condition may give indications on water level and hence rewetting success. We mapped the fractions of seven peatland related and four non-peatland vegetation classes, as well as their dynamics in condition from five 30 m EnMAP images. We used neural network regression with synthetic training data augmentation to predict peatland vegetation fractions (e.g., *Phragmites australis*, *Typha* spp. and *Carex* spp.) from the hyperspectral EnMAP stack, as well as NPV (non-photosynthetically active vegetation), GV (green vegetation), and water fractions from the single-dates to derive intra-annual dynamics. Patterns of species fractions matched field observations at varying accuracies with the highest agreement for Typha and Phragmites (MAE = 16% and 22%, respectively). The changes in vegetation condition similarly matched field observations (GV: MAE = 12%, Water: MAE = 14%, NPV = 21%), and in combination with species fractions revealed class-specific trends, such as differences in timing of the green peak (maximum GV fractions). Intraspecific variations in green peak could be observed for the class Phragmites, indicating differences in water level. Further, dynamics in the extent of open water areas were apparent, highlighting the necessity of multi-temporal information. Increasing availability of spaceborne imaging spectroscopy will enable long-term monitoring of peatland rewetting, accounting for intra-annual variations in vegetation and water dynamics.

KEYWORDS
EnMAP, hyperspectral, NPV, peatland rewetting/restoration, *Phragmites australis*, regression based unmixing

1 Introduction

Peatlands are wet ecosystems comprising water saturated organic soils that act as large carbon stocks (450–650 Gt) (UNEP, 2022). Approximately 12% of global peatland cover has been subject to drainage practices leading to environmental degradation (Tanneberger et al., 2009; Zak et al., 2010; Erkens et al., 2016) which contributes 4% of global annual total GHG (Greenhouse Gas) emissions (UNEP, 2022). In Germany, drained organic soils are responsible for up to 7% (UBA, 2022), and in the federal state of Mecklenburg-Western Pomerania even up to 40% of its annual emissions (Uellendahl et al., 2023). Peatland

rewetting and restoring is therefore crucial in mitigating climate change (Mrotzek et al., 2020; Günther et al., 2020).

Rewetted peatlands differ from their natural counterparts in both abiotic and biotic factors (Kreyling et al., 2021). Drainage reduces the characteristic self-regulatory capacity of natural peatlands by altering the soil structure. This may lead to higher water level fluctuations but also promotes inundation after rewetting (Kreyling et al., 2021; Liu and Lennartz, 2019), and consequently increased GHG emissions (Hahn et al., 2015; Franz et al., 2016; Tiemeyer et al., 2016). These rewetted peatlands are also more susceptible to extreme weather events, such as droughts, which may further elevate GHG emissions (Koebsch et al., 2020). Continuous monitoring of rewetted peatlands is therefore invaluable to track adequate water levels and vegetation development as proxy for GHG emissions and degradation (Minasny et al., 2023; Waard et al., 2024).

In north-east Germany, driving factors of vegetation development after rewetting are the spatial variability of water table depth and nutrient availability (Zerbe et al., 2013). These factors have led to the development of a mosaic and the dominance of tall helophytes, such as *Typha latifolia*, *Phalaris arundinacea*, *Phragmites australis*, and *Carex* spp. (Kreyling et al., 2021; Zerbe et al., 2013, see Figure 1). *P. australis* and *T. latifolia* are commonly found on permanently inundated sites and are known to thrive under nutrient rich conditions (Vroom et al., 2018; Geurts and Fritz, 2018), while *Carex* spp. show varied responses to water level but tend to grow in soils prone to seasonal water level fluctuations (Edwards et al., 2025; Lawniczak et al., 2010; Schulz et al., 2011). *P. arundinacea,* mainly a remnant of pre-rewetting condition, grows under the comparably driest conditions but tolerates flooding (Jensen et al., 2024; Frick et al., 2011).

In addition to species occurrence, the presence of non-photosynthetically active vegetation (NPV) and photosynthetically active, green vegetation (GV) can serve as an indicator for the water regime. In peatlands, NPV can be mainly found in the remaining standing biomass from the previous vegetation period, or as senescent foliage and flowers from the current year. The presence of senescent foliage can be species-specific and vary over time, e.g., *Carex* spp. emerge early in the season while *P. australis* shoots emerge comparably late (Figure 2, left). Variations in NPV shares can even occur within the same species (Figure 2, right), probably due to differences in microclimate and topography or genetics (Verrelst et al., 2023; Feilhauer et al., 2013; Kuprina et al., 2025). As an example, droughts resulted in a reduction in NDVI (normalize difference vegetation index) of boreal peatland vegetation, due to an increased share of senescent foliage (McPartland et al., 2018). This stresses the importance of interannual, species-specific NPV and GV variations, as well as extent and frequency of inundated areas for understanding rewetting effects.

Maps on species abundance and vegetation condition from remote sensing may serve as a proxy for water level and hence contribute to assessing the effects of rewetting. So far, multispectral spaceborne and airborne data was often used to map peatland extent (Pflugmacher et al., 2007; Krankina et al., 2008), peatland vegetation types (Räsänen and Virtanen, 2019; Steenvoorden and Limpens, 2023) and peatland species (Frick et al., 2011) at varying spatial resolutions. However, hyperspectral information promises great opportunities in peatland vegetation mapping and quantification due to capturing the distinct cellulose and lignin absorption features in the SWIR (shortwave infrared) region at 1,730 nm, 2,100 nm and 2,300 nm (Cole et al., 2014; Elvidge, 1990). Field spectroscopy was used in peatland vegetation research (Pang et al., 2022; Salko et al., 2025; McPartland et al., 2019; Salko et al., 2024). Salko et al. (2025) successfully predicted the fraction coverage of NPV (litter) from spectroscopy data, but its spatial coverage and transferability are limited. Airborne hyperspectral data has been used in mapping plant traits, gradients and the extent of *P. australis* over larger areas (Feilhauer et al., 2011; Harris et al., 2015; Kattenborn et al., 2017; Middleton et al., 2012; Elmer et al., 2021), but airborne campaigns are resource intensive and restricted to single regions and dates. Still, studies using spaceborne imaging spectroscopy data, at the cost of low spatial resolution, in peatland vegetation mapping are scarce (e.g., Arasumani et al., 2023).

Various studies have shown that multi-temporal data is invaluable for vegetation mapping because of the information inherent in vegetation phenology (Dudley et al., 2015; Arasumani et al., 2023; Pang et al., 2022) proposed using multi-temporal data when possible, because ideal dates may vary between climate zones, peatland types, and sites (Cole et al., 2014; Feilhauer and Schmidtlein, 2011). Further, peatland species distribution and their condition are driven by water availability, which varies in the course of the year. Arasumani et al. (2023) demonstrated that multi-temporal hyperspectral PRISMA data improves vegetation mapping accuracy on peatlands, highlighting the importance of hyperspectral time series observations. However, in this case, multi-temporal observations were used to improve species mapping accuracies rather than monitoring changes in vegetation phenology throughout a year. Existing products and initiatives, such as the Copernicus Water and Wetness product (https://land.copernicus.eu/en/products/high-resolution-layer-water-and-wetness) and the Global Wetland Watch (https://map.globalwetlandwatch.org/), provide valuable information on wetland ecosystems, but these often offer aggregated data over broader temporal scales and may overlook the specific dynamics of peatlands. Ongoing and upcoming hyperspectral satellite missions (PRISMA, EnMAP, SBG, CHIME), will increase data availability and open new opportunities to map large-scale inter- and intra-annual vegetation phenology, water level fluctuation and inundation. Therefore, we want to assess the potential of the recently available EnMAP data (Environmental Mapping and Analysis Program, Storch et al., 2023), with its high spectral resolution and potentially high temporal resolution, for monitoring rewetted peatlands.

Current vegetation studies using EnMAP data mainly covered dry biotopes, such as Namibian grasslands (Bantelmann et al., 2024) or the Atacama Desert (Reddig et al., 2025) or croplands, to map crop traits (e.g., Flynn et al., 2026; Yilmaz et al., 2026). Unlike croplands and dry habitats, where spectral signatures are largely shaped by soil properties, peatland reflectance depends on water, peat, and low growing vegetation, introducing additional complexity. Therefore, assessing the suitability of EnMAP imagery with intra-annual information for wetland ecosystems is essential.

The sensor offers a 30 m spatial resolution, which risks simplifying the small-scale heterogeneity of peatland vegetation in discrete mapping schemes, but the high spectral resolution of 246 bands allows for a deeper insight into subpixel processes. To

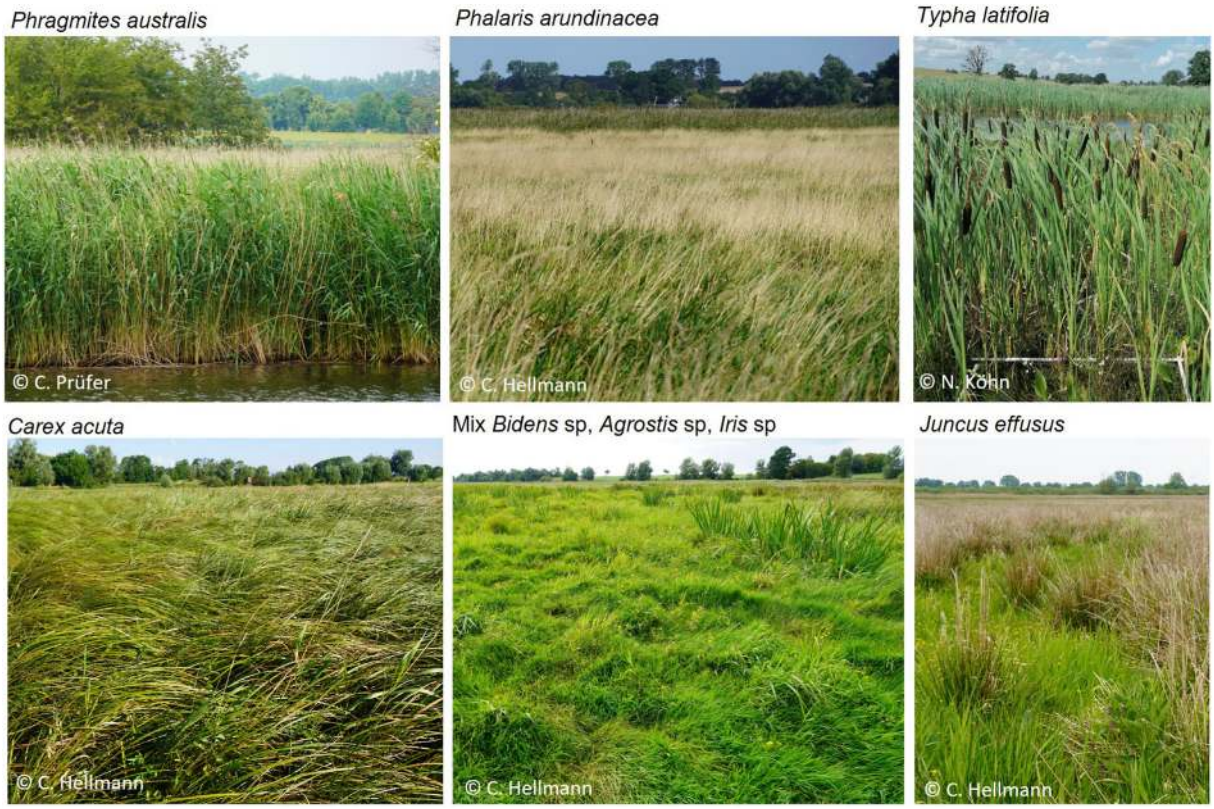


FIGURE 1
Different fen peatland species in rewetted peatlands of Mecklenburg-Western Pomerania. *Phragmites australis*, *Phalaris arundinacea*, *Typha latifolia* and *Carex acuta* grow in dominant patches. *Bidens cernua*, *Agrostis stolonifera*, and *Juncus effusus* often grow intermixed.

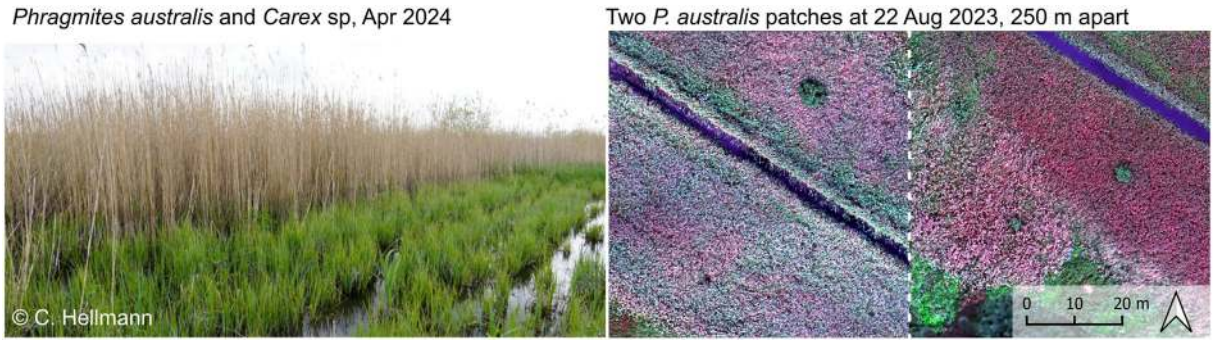


FIGURE 2
Left: *Phragmites australis* and *Carex* sp at the same time in April 2024. *P. australis* consisted of mainly dead shoots/aboveground biomass, while *Carex* sp was already green. Right: *P. australis* in RGB UAV imagery visually in different senescent stages at the same point in time and only 250 m apart.

derive information at sub-pixel scale we used a regression-based unmixing approach for fraction mapping using synthetic training data (Okujeni et al., 2017; Okujeni et al., 2013), as this approach has proven useful in vegetation studies covering various ecosystems (Cooper et al., 2020; Reddig et al., 2025; Mandl et al., 2024; Arasumani et al., 2023). Kowalski et al. (2022) and Kowalski et al. (2023) successfully modelled fractions of NPV, GV and soil with this approach for drought monitoring in Central European grasslands. Further, Lobert et al. (2025a) quantified year round cropland cover and revealed spatio-temporal patterns of winter cropland cover in Germany (Lobert et al., 2025b).

While most of these studies had a focus on rather homogenous and comparably dry land cover types, we adapted the unmixing approach to a landscape with heterogenous and wet peatland ecosystems and assessed the suitability of multi-temporal EnMAP data to map intra-annual vegetation and water dynamics in the

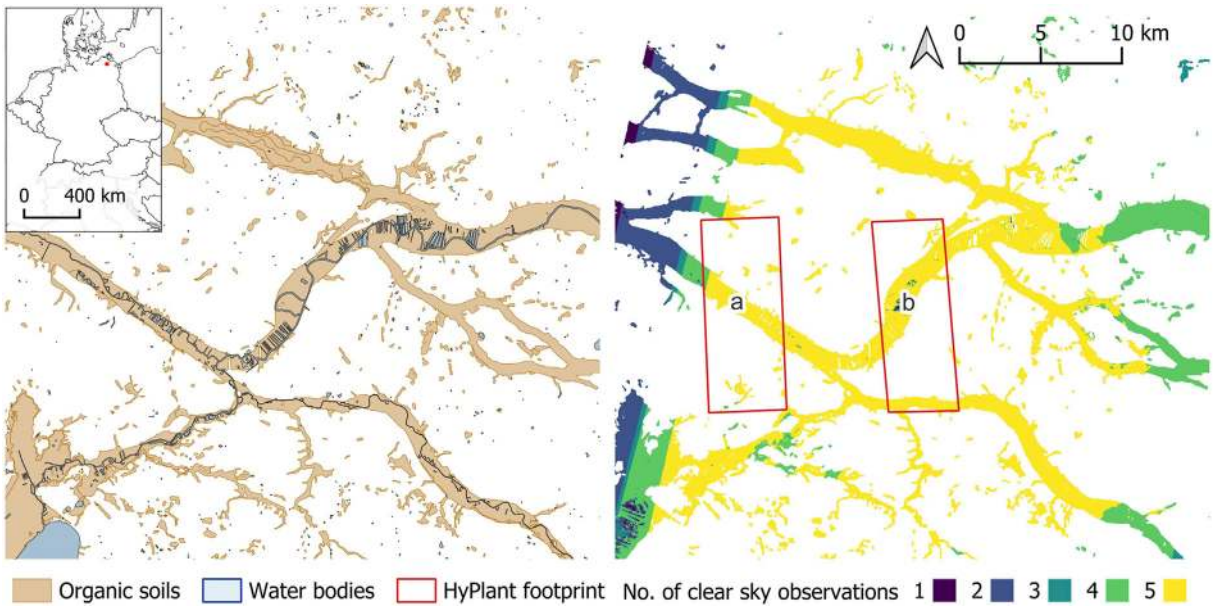


FIGURE 3
Overview of the study area in north-eastern Germany. The area of interest is reduced to organic soils (Wittnebel et al., 2023) (left). Five EnMAP observations were available from 2022 to 2025 (right). Pixels of five observations were used, excluding clouds and single observations. Airborne HyPlant imagery was acquired for two subset areas (a, b). Sources: European country boundaries were derived from Eurostat (https://ec.europa.eu/eurostat/web/gisco/overview). Water bodies were derived from Open Street Map.

context of peatland rewetting in north-east Germany. More specifically, we asked the following research questions:

1. How accurately can we map dominant peatland species using multi-temporal EnMAP data?
2. How accurately can we map intra-annual variability in vegetation phenology and water inundation at a subpixel scale using multi-temporal EnMAP data?
3. Can we observe variations in phenology patterns between or within dominant peatland species?

To answer these questions, we first implemented regression based unmixing with synthetic training data to predict fractions of dominant peatland species from a multi-temporal EnMAP data stack comprising five observations. We then quantified fractions of NPV, GV and water for each EnMAP observation, individually. In a last step, both products were combined to derive phenological trends for dominant peatland vegetation as an indicator for water level.

2 Materials and methods

2.1 Study area

The study area is located in north-east Germany, in the federal state of Mecklenburg-Western Pomerania. The climate is temperate with annual precipitation of 538 mm and a mean air temperature of 9.2 °C (1991–2020) at the nearest weather station in Teterow (Deutscher Wetterdienst, 2025). The main peatland types found in this region are percolation mires fed by groundwater and close to the Peene and Trebel rivers (Figure 3) (Succow and Jeschke, 1986). The peatlands in the Peene and Trebel river valleys were largely drained during the 19th century for peat extraction and agricultural purposes but many of the peatlands underwent rewetting around the year 2000 (Zerbe et al., 2013). After rewetting, a mosaic of tall helophytes, such as *Typha latifolia* and *Phalaris arundinacea*, *Phragmites australis*, and *Carex* spp. developed (Figures 1, 2). The study area was restricted by EnMAP coverage to a 30 km × 50 km area (Figure 3), but these vegetation patterns are characteristic of European fen peatlands (Kreyling et al., 2021; Zerbe et al., 2013).

2.2 Satellite imagery

We used EnMAP data for mapping quantitative peatland vegetation types and vegetation condition. All clear (clouds less than 10%) EnMAP L2A data for the given region (five dates within 2023–2025, Figure 3; Supplementary Table A) were downloaded via the data access portal. Additional data preparation was necessary (Figure 4). Clouds were masked as described in Wright et al. (2025) due to inconsistencies of the provided cloud mask. The images were co-registered to Landsat mean composites of ±30 days around each EnMAP scene using AROSICS (Scheffler et al., 2017) to improve spatial alignment between all scenes. The NIR bands in the NIR-SWIR sensor overlap region and bands affected by atmospheric noise were removed reducing the number of bands from 246 to 195. The EnMAP data was ordered by day of year instead of absolute chronology, i.e., 26 April (2025), 02 May (2024), 02 June (2023), 18 August (2023), and 22 September (2024), to represent intra-annual phenological variability. Sun elevation varied from

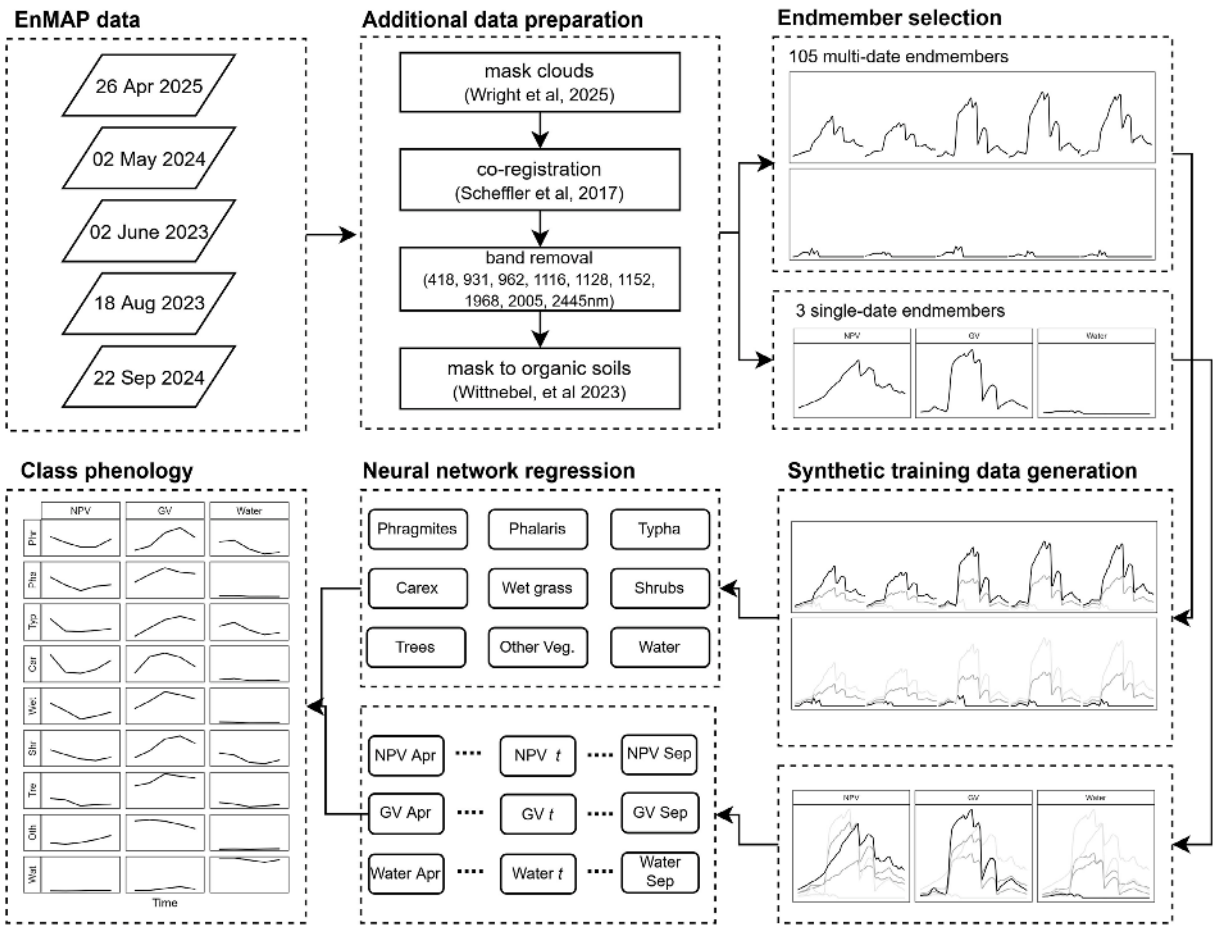


FIGURE 4
Workflow. EnMAP data preparation included cloud masking, co-registration to Landsat mean composites of ±30 days around each EnMAP scene, removal of noisy bands and masking to the Organic Soils. Spectral input for synthetic training data generation was based on the stacked imagery for the species but only single dates for the NPV-GV-Water endmembers. Model prediction for the species was then applied to the stacked data, and NPV-GV-Water separately for each date. Class specific phenology was derived from the combination of those two products.

approximately 49°–59° across the five acquisition dates, except for the September acquisition, where it was 36° (Supplementary Table A). The analysis was restricted to the boundaries of the Organic Soils mask (Wittnebel et al., 2023).

2.3 Regression based unmixing

Subpixel fractions were predicted using regression based unmixing, a methodology successfully used in diverse vegetation studies across various ecosystems and climate. Recent studies covered temperate grasslands (Kowalski et al., 2022; Kowalski et al., 2023) and croplands (Lobert et al., 2025a; Lobert et al., 2025b), subalpine forests (Mandl et al., 2024), arctic shrublands (Nill et al., 2022), woody vegetation in a temperate and Mediterranean climate but also temperate peatlands (Arasumani et al., 2023). Further, large-scale land cover and land use changes were mapped by Stanimirova et al. (2022) using this method, and Okujeni et al. (2018) and Suess et al. (2018) have demonstrated its spatial and temporal transferability. The variety of the studies showcase the suitability of the regression based unmixing method for our analyses.

Since this method requires extensive training data, we used synthetic training data generation from pure pixels (Okujeni et al., 2013; Priem et al., 2019; Figure 4). For training data generation, pixels of each class representing a fraction cover of 100% ("endmember") were selected. The spectral profiles of the pure pixel endmembers were then used as input for synthetic mixing. The spectra are linearly combined, and weighted by randomly assigned fractions, with the constraint of summing to 1 (Pham et al., 2024). The synthetic training data can serve as input for various machine learning algorithms (Lopatin et al., 2016; Mandl et al., 2024; Reddig et al., 2025). Here, we used a multi-class Neural Network Regression to allow for multi-class regression (Specht, 1991), as proposed by Pham et al. (2024).

2.3.1 Endmember selection species fractions

The final selection of class-wise training data to quantify peatland species abundance was based on dominant vegetation patches found in the area of interest. Although some peatland related classes may comprise different species, we refer to this approach as species mapping. The endmembers were manually

10.3389/fenvs.2026.1805563

TABLE 1 Species mapping target classes and number of selected endmembers (n).

Peatland relation	Class	Species/Groups	n
Peatland related	Phragmites	*P. australis*	10
	Typha	*T. latifolia*, *T. angustifolia*	8
	Carex	*C. acutiformis*, *C. riparia*, *C. acuta*	11
	Phalaris	*P. arundinacea*	4
	Wet grassland	*Bidens cernua*, *Agrostis stolonifera*, *Juncus effusus*, *Iris pseudacorus*	6
	Shrubs	Mainly *Salix* spp.	19
	Water	Permanent water	6
Non-peatland related	Trees	Deciduous and needle-leaf trees	14
	Other vegetation	Cropland and managed grassland	20
	Artificial	Urban settlements	7

selected for single species, groups of species and groups (Table 1). The classes Phragmites, Typha, Carex, and Phalaris occasionally appeared in patches larger than single pixels (30 m × 30 m). The Wet grassland class included a mixture of non-dominant peatland vegetation (Figure 1) but can also grow intermixed with the previous mentioned classes. Phalaris and Wet grassland had the smallest sample, since large, homogeneous patches were scarce. A permanent "Water" class was included (at least four out of five times water) to separate permanent water from dynamic water changes. Dynamic changes in water area were then considered from the interannual NPV-GV-Water fractions. The class "Artificial" is rare within the Organic Soils mask and mainly found at the edges as urban settlements. Spectral variability within each class had to be considered during endmember selection, e.g., different species for Wet grassland or Carex. The regression based unmixing approach has been shown to be capable of dealing with multi-modal and heterogeneous classes (Cooper et al., 2020; Schug et al., 2020). As such, remaining vegetation types were grouped in the class Other vegetation, i.e., croplands and mown grasslands. Croplands and grasslands exhibit variations in timing of harvesting and mowing events, which had to be considered in the endmember selection.

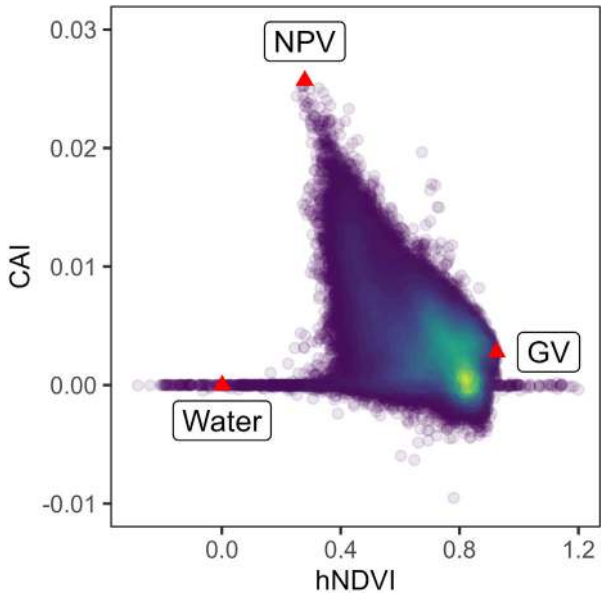


FIGURE 5
CAI–hNDVI feature space based on 63,221 pixels from typical rewetted peatlands, for all dates. The location of the final endmembers were marked with a red triangle. 35 points are located outside of this plot and were ignored (low CAI from solar panels close to peatlands, very high hNDVI > 50 over water).

2.3.2 Endmember selection NPV-GV-Water fractions

The endmember selection for NPV, GV and Water was inspired from recent studies (Kowalski et al., 2022; Tian et al., 2023) based on Guerschman et al. (2009) in which pure endmembers (i.e., GV, NPV and soil) are located at the vertices of a triangular feature space using two different indices (commonly NDVI versus SWIR). Our adapted methodology replaces soil with water and constructs the feature space using hNDVI (hyperspectral Normalized Difference Vegetation Index, Oppelt, 2002) versus CAI (Cellulose Absorption Index, Nagler et al., 2000) as proposed by Guerschman et al. (2009). The hNDVI is an adaptation of the NDVI, a commonly used vegetation index to hyperspectral data, and CAI is a common index in NPV cover estimation from imaging spectroscopy data (Daughtry et al., 2004; Nagler et al., 2003). The feature space (Figure 5) was built from representative peatland areas (63,221 pixels, from all dates) with typical peatland vegetation types, excluding trees and shrubs (Kowalski et al., 2023). The final NPV endmember was selected for maximum CAI, and the GV endmember for maximum hNDVI value. The Water endmember was selected as the pixel closest to 0 for both indices. Water showed unrealistic hNDVI values, ranging from negative values up to values larger than 1. A simple threshold was used to separate Water from the final GV endmember (reflectance at 1,211 nm > 0.2). The final pixels were manually investigated for representativeness and homogeneity.

2.3.3 Spectral library and synthetic training data

Two different spectral libraries were built from the endmembers. For the species endmembers (Supplementary Figure A), the spectral information was based on multi-temporal information, i.e., the stacked EnMAP imagery. The input image varied for the NPV-GV-Water endmembers (Supplementary Figure B), based on the timing of maximum GV, NPV and water fractions (i.e., June, April, and May, respectively).

Using the pure endmember spectral profiles, we generated synthetically mixed spectra with multi-label information following the spectral mixing approach described by Okujeni et al. (2013) and the workflow proposed by Pham et al. (2024). The procedure consisted of the following steps:

1. Endmember selection: We randomly selected 2, 3, or 4 pure endmember pixels from the endmember pool (endmembers from the same class could be selected multiple times).
2. Fraction assignment: We assigned a random fractional abundance between 0 and 1 to each selected endmember, with the constraint that the fractions summed to 1.
3. Synthetic data: We generated the synthetic spectra as the linear combination of the selected endmember spectra weighted by their assigned fractions. The resulting synthetic spectra were used as input features (Figure 4), and the corresponding fractions served as regression targets for training a multi-class regression model.

In this study, we developed two models: one for the species fractions with ten classes and one for NPV-GV-Water fractions with three classes. For each model, we generated 128,000 synthetic training samples following the recommendation of Pham et al. (2024). These samples were used to train multi-class Neural Network Regression (NNR) models. The input data had a two dimensional shape (X1, X2), where X1 denotes the number of EnMAP spectral bands and X2 represents the number of acquisition dates in the EnMAP stack. The NNR architecture comprised two hidden layers with 512 neurons each. The output layers contained 10 and 3 units, corresponding to the predicted fractions of the 10 and 3 target classes for each model, respectively. Model parameters were optimized using the L1 loss function (mean absolute error) during training. For more detailed information we refer to the Supplementary Tables B,C.

All analyses were undertaken with R (v4.2.2, R Core Team, 2022) using the packages *terra* (v1.8, Hijmans, 2025). Synthetic training data generation, and NNR training and the classification of HyPlant data for validation were done with python using PyTorch.

2.4 Validation

The EnMAP species maps were validated with species fractions derived from airborne imaging spectroscopy data (HyPlant), while UAV derived NPV-GV-Water fractions were used to validate the EnMAP NPV-GV-Water maps. RMSE, MAE and scatterplots with a fitted linear regression, as well as visual interpretation of the maps, were used for validation. As observed by Reddig et al. (2025), the high number of classes and class-wise scarce occurrences resulted in a high density of predicted fractions close to 0. To avoid a positive bias of the validation metrics, the metrics were calculated from a random subset of the complete data set for all species classes and NPV-GV-Water fractions. For this, the HyPlant- and UAV-derived fractions were grouped into 10-percent bins, and for each bin the maximum sample (35 for HyPlant and 51 for UAV) was randomly drawn (e.g., 35 samples within 0%–10%, 35 within 11%–20%, etc.). We repeated this process 100 times to avoid random effects and from all 100 random draws, a mean fitted linear regression, R^2, RMSE and MAE values were calculated (Supplementary Table D). Since the deviation between the 100 random draws were small, we show and discuss MAE, and RMSE values for one random subset. Although our validation utilizes classifications from high spatial resolution imagery instead of direct field measurements, it could be considered verification, but this approach is not uncommon (Gray et al., 2018; Tian et al., 2023; Reddig et al., 2025).

2.4.1 HyPlant species fractions

EnMAP species fractions were validated using a discrete classification of imaging spectrometer data from the airborne HyPlant imaging spectrometer (Rascher et al., 2015). Acquisition date was 27 August 2024; spatial resolution of the imagery from the broad band dual channel (380–2,500 nm) was 2.6 m. The top-of-canopy reflectance was calculated according to Siegmann et al. (2019). The LiDAR (RIEGL Laser Measurement Systems GmbH, Austria) sensor was flown in parallel providing a digital terrain model (DTM) and digital surface model (DSM). A normalized DSM (nDSM) was calculated and used in the classification process.

Wetland, non-wetland and water land cover classes were first separated in a general classification by combining the Google Satellite Embeddings (Brown et al., 2025) dataset in 2024 with the HyPlant data and nDSM. Detailed classifications within each of the general classes were then performed using only the HyPlant data and nDSM, separated by the subset areas. Both classification steps utilized a three-model ensemble of neural networks with three hidden layers. Training, validation, and test data, derived from manual labelling and expert knowledge, was randomly split three times and the majority voted value per pixel was assigned as the output. The final outputs combined the classifications within the wetland and non-wetland groups, and water from the general classification. Species fractions were calculated from a resampled HyPlant classification to match the EnMAP grid.

2.4.2 UAV NPV-GV-Water fractions

Multispectral UAV acquisitions were undertaken within 6 days of the EnMAP acquisitions for two subplots in region b (Figure 3). The usage of an RTK (real-time kinematic) base station and SAPOS® (https://sapos.de/) for precise real-time positioning resulted in an XY-accuracy of 3 cm (based on 21 ground control points). Detailed information on the sensors and mission settings are summarised in Table 2. Speed and overlap varied between the two drones. Image pre-processing was done in Pix4DMapper (v4.9.0) and Agisoft Metashape Professional (v1.8.4 and v2.1.3).

The final eight orthomosaics were used in their original resolution (3 cm–6 cm) and a discrete classification scheme.

TABLE 2 Information on UAV sensors and mission settings.

UAV	Type	Sensor	Center wavelengths	Acquisition dates	Height [m above starting point]	Speed [m s^{-1}]	Front overlap [%]	Side overlap [%]
DJI M300	Quadrocopter	Altum-PT (MicaSense)	475 nm (Blue), 560 nm (Green), 668 nm (Red), 717 nm (Red edge) and 842 nm (Near Infrared)	25 April 2025 08 May 2024 08 June 2023 22 August 2024	70–80	5	80	70
Trinity F90+	Fixed wing	RedEdge-M (MicaSense)	475 nm (Blue), 560 nm (Green), 668 nm (Red), 717 nm (Red edge) and 842 nm (Near Infrared)	20 September 2024	70–80	Approx. 16	62	80

Manual decision trees were built for each orthomosaic to predict NPV, GV and Water. Shadow was treated as water, and open peat was treated as NPV, since it comprised dead organic plant material, and was spectrally similar to NPV when dry. A random subset was drawn of 50 points for NPV and GV and 15 points for Water and each orthomosaic for a separate validation. Each point was visually assessed and assigned to one of the three classes. The overall accuracy ranged from 76% to 95% and F1 scores of 73%–100%. The classifications were resampled to the EnMAP grid while calculating the respective fractions of NPV, GV and Water.

3 Results

3.1 Species fractions

The species maps show heterogeneous vegetation patterns. Phragmites was the most dominant, often found along river edges and open water bodies in linear, narrow structures, but some dominant clusters were also visible. Carex and Typha were mapped in large patches. A visual comparison of the distribution of the three classes (Figure 6) reveals a good agreement with the HyPlant fractions, despite some inconsistencies in the distribution of Typha with overestimation of low fraction values.

Of the peatland related classes, Typha showed the highest accuracy (MAE = 16%, RMSE = 20%), with decreasing accuracy for Phragmites, Carex, and lowest accuracies for Phalaris and Wet grassland (MAE = 22–42%, RMSE = 28–51%, Figure 7). Shrubs, Trees and Water showed matching distribution patterns in the validation plots (MAE = 18–19%, RMSE = 22–25%, Supplementary Figure C).

3.2 NPV-GV-Water fractions

Similar to heterogenous species distribution patterns, peatlands showed heterogeneous phenology patterns over the course of a year. April had the highest fractions of NPV, June and August showed the lowest NPV fractions but in turn the highest GV fractions. Further, mapped Water fractions were high in April and May but low in June and August (Figures 8a,b).

Different phenological trends were visible from the spectral information and fraction maps, such as early greening (Figure 8c) with strongest vegetation signal in June and a flooding event observed in May, which was typical for areas with Carex. Late greening was observed, e.g., for Phragmites, with strongest vegetation signal in August. Other vegetation, such as croplands and managed areas showed pronounced changes in GV and NPV fractions. These trends do not represent a single year, as data from multiple years were treated as one. Permanent open water bodies showed high water fractions throughout the observation period (Figure 8c).

Scatter plots with UAV derived validation data on NPV, GV and Water fractions showed the highest accuracy for GV (MAE = 12%, RMSE = 16%) and lower accuracies for Water and NPV, respectively (Figure 9). NPV and Water were often confused where wet or dry peat was mapped as Water in the EnMAP fractions but NPV in UAV imagery, especially in May and June. Therefore, when discussing phenological trends, GV trends should be considered more reliable than Water and NPV which need to be discussed with care.

3.3 Species phenology

By combining the species and NPV-GV-Water fraction maps, variation in phenology between species became apparent. The peatland classes showed varying trends, such as late greening of Phragmites (Figure 10). Also, small-scale patterns of temporal variations in the timing of maximum GV values were visible for Phragmites (Figure 11). Carex showed early greening while Typha displayed a general steady increase in GV (Figure 10). Phalaris and Wet grassland shared similar trends, although they had the lowest mapping confidence and should be discussed cautiously. Other vegetation showed the highest GV fractions but also large deviations of GV and NPV, potentially due to differences in management strategies.

The Water class from the species mapping included permanent open water bodies. As such, the water fractions were generally high over the course of the vegetation period and the change in water fractions small. Although a green peak in August was observed coming from dried up edges of open water bodies and lake like structures with vegetation growth. In turn, the change in Water

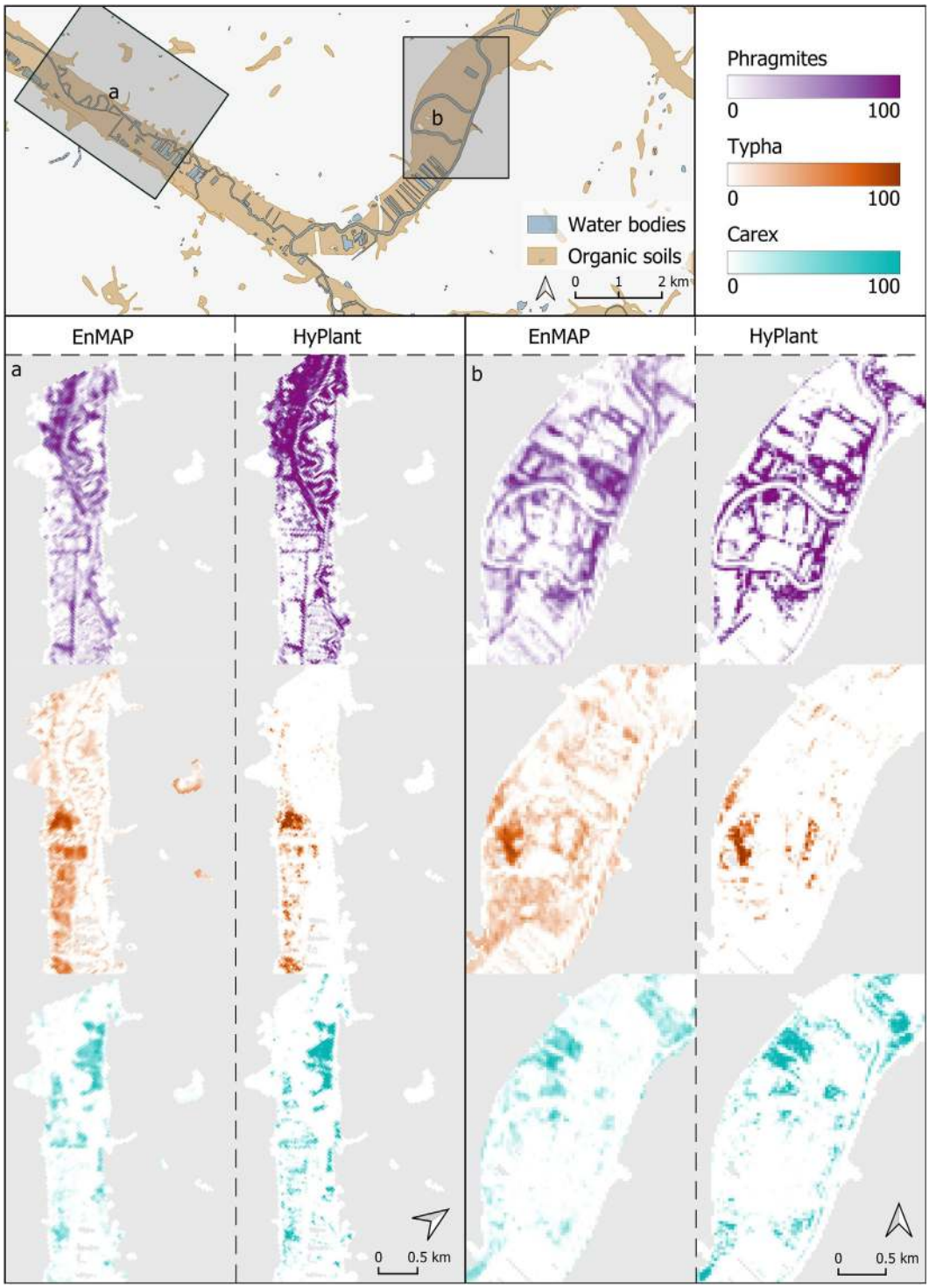


FIGURE 6
Species fractions for EnMAP and HyPlant and three exemplary peatland classes (Phragmites, Typha and Carex). The location of the subset regions a and b are shown in the top left. Grey color: outside of the organic soils (Wittnebel et al., 2023). Water bodies were derived from Open Street Map..

fractions over time varied between the species classes. Phragmites, Typha, Shrubs and Trees showed similar trends with high water fractions at the beginning of the season but a decrease over time. In contrast, Carex, Phalaris, Wet Grassland, and Other vegetation showed less inundation overall.

4 Discussion

We were successful in using multi-temporal EnMAP data for mapping dominant peatland species and intra-annual vegetation and water dynamics. By using a multi-temporal hyperspectral data

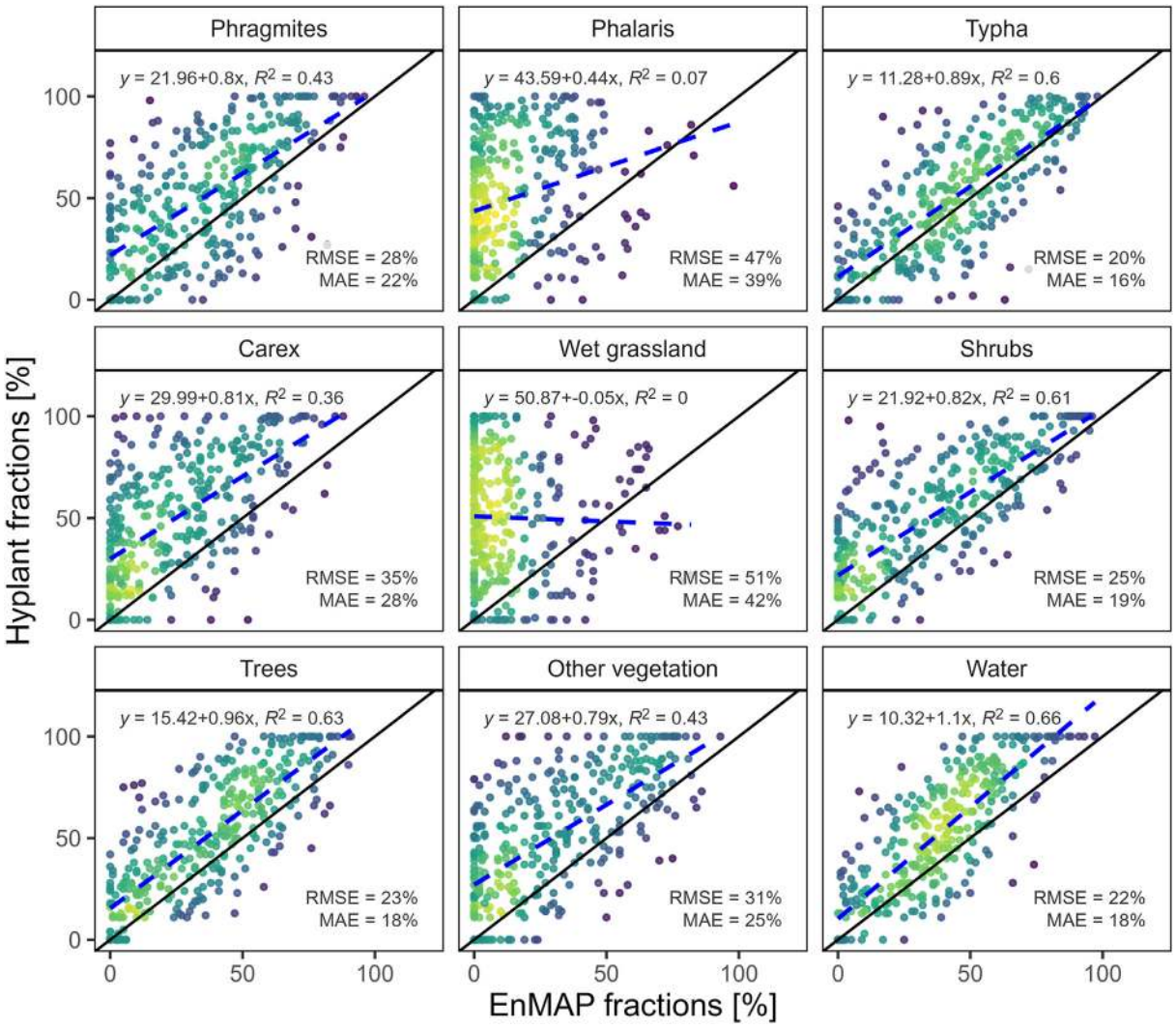


FIGURE 7
Validation scatterplot for a random subset. A subset was randomly drawn for each class and 10-percent bin of the HyPlant data. Blue dashed line = regression line for the random sample. Black line = 1:1 line. Color scale indicates data density: blue = low density, yellow = high density.

stack, we leveraged the class specific phenological variation for species mapping. NPV, GV and water fractions were predicted for each date, which in combination with the species fractions revealed distinct phenological trends for the different dominant peatland vegetation types.

4.1 Species fractions

The mapped species fractions generally matched the observed spatial patterns. Phragmites and Carex were mapped with moderate confidence (MAE = 22–28%), but their spatial extents corresponded well with observed patterns (Figure 6). Typha was mapped with smaller errors (MAE = 16%) where it was the dominant species (approx. > 70%), but was substantially overestimated where it was sparse or absent, particularly in areas of high water-level fluctuation. Phalaris and Wet grassland showed no correlation between predicted and observed fractions (R^2 = 0–0.07), potentially due to the inherently rare occurrence of both classes in our study area, which limited the availability of representative endmember samples. For the class Water, six endmembers were sufficient representative to achieve good accuracies (n = 6, R^2 = 0.66, MAE = 18%). Similarly, Okujeni et al. (2013) showed good performance for the grass class with only a small number of sample size (n = 5), although the study was based in urban context and the only other vegetation class was trees. In other mapping studies, greater numbers of endmembers were used (Cooper et al., 2020; Okujeni et al., 2018; Mandl et al., 2024; Reddig et al., 2025). In the case of Phalaris and Wet grassland, the low number of samples (n = 4 and 6, respectively) appears small given the spectral variance within and spectral similarity between the two classes (Supplementary Figure A). This limitation likely increased confusion, however the use of synthetic training data relies on pure pixel endmembers, which in this case can hardly be found.

While Arasumani et al. (2023) reported better MAE values (14%–20%), our study included a greater number of vegetation classes (eight, to our knowledge the largest used with regression-

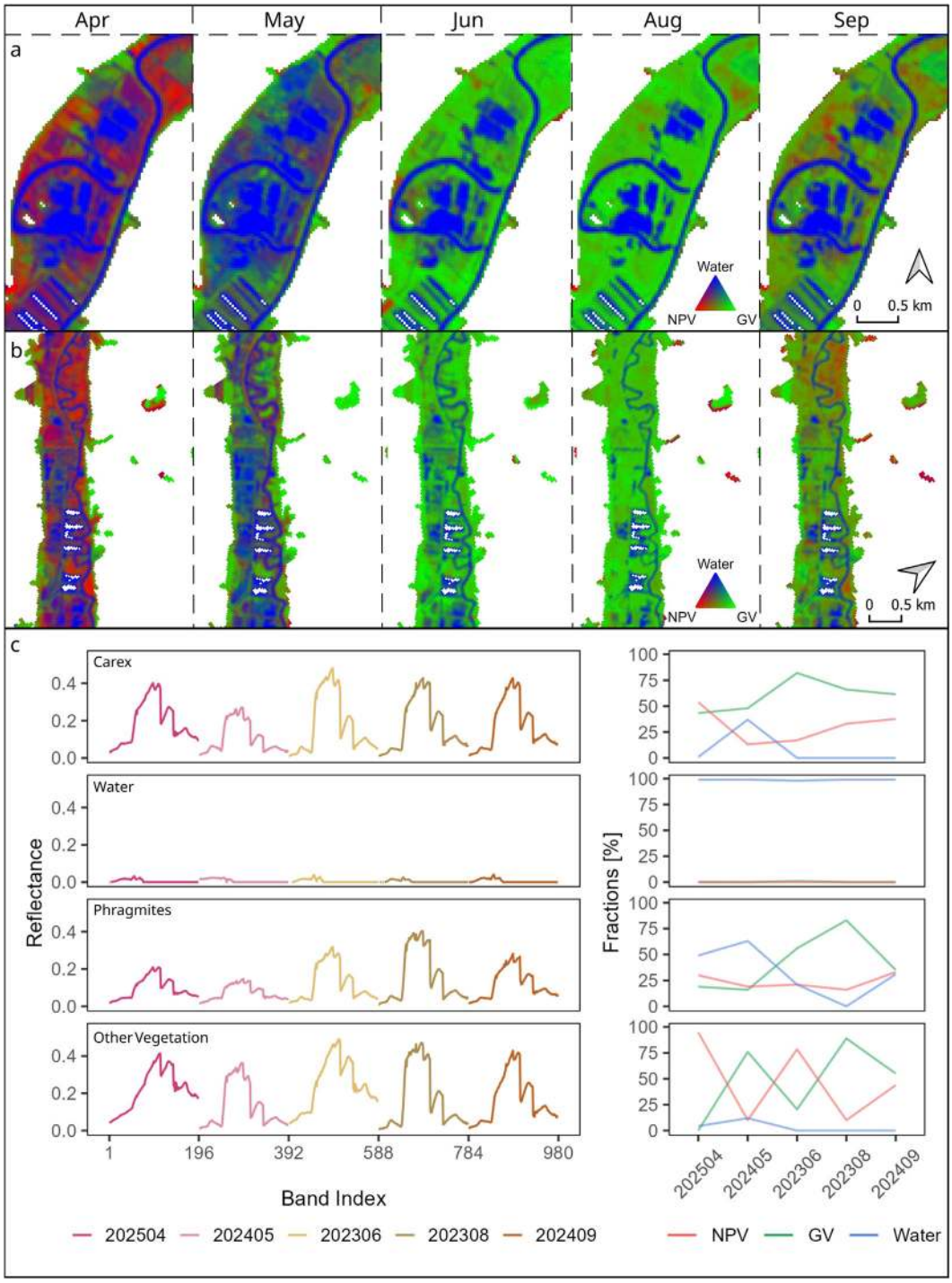


FIGURE 8
(a, b) NPV, GV and Water fractions over the course of the year for the same subset areas as in Figure 6. In white, areas outside of the organic soils (Wittnebel et al., 2023). **(c)** Spectral change of four exemplary pixels representing dominant vegetation types and their respective phenological development derived from NPV-GV-Water fractions over the course of the year, sorted by month. For the visualization of the spectra, the images were stacked and the band names indexed.

based unmixing, so far). This increased complexity likely contributed to higher MAE values due to potential class confusion. Salko et al. (2025) similarly showed variable performance in species fraction predictions from field spectroscopy data for six peatland species, underlining the challenges of peatland vegetation mapping. Mapping multiple, spectrally similar vegetation classes in peatlands therefore differs from previous mapping applications that typically involve fewer classes or more general land cover types (Reddig et al., 2025; Cooper et al., 2020). Integrating Synthetic Aperture Radar (SAR) data to

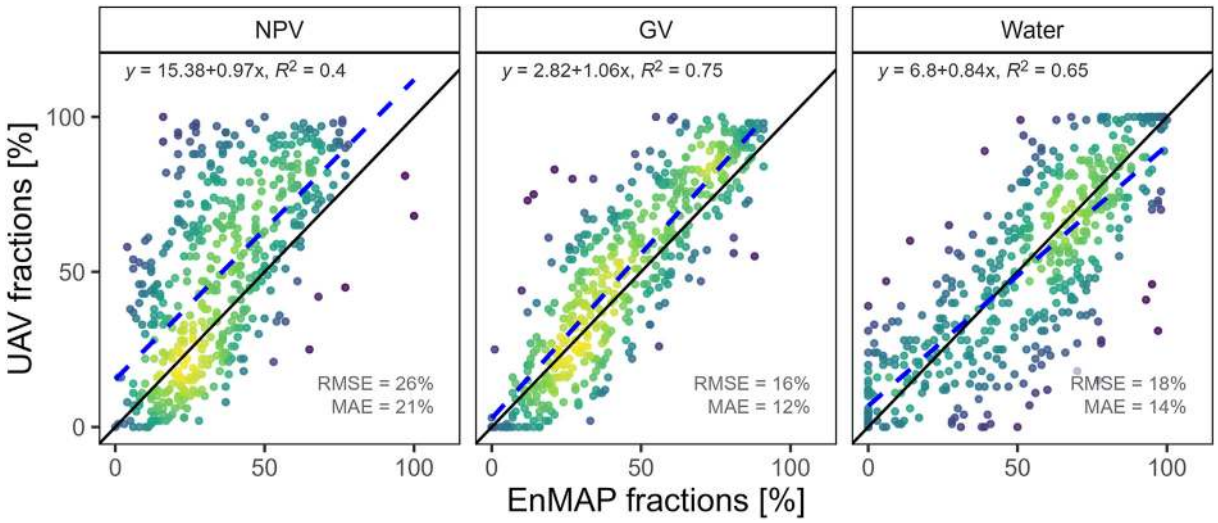


FIGURE 9
Validation scatterplot for GV–NPV–Water fractions. A subset was randomly drawn for each class and 10-percent bin of the HyPlant data. Blue dashed line = regression line for the random sample. Black line = 1:1 line. Color scale indicates data density: blue = low density, yellow = high density.

incorporate textural information could improve class separability (Dąbrowska-Zielińska et al., 2012; Dabrowska-Zielinska et al., 2014), though adapting the current spectral unmixing methodology would be necessary.

4.2 NPV-GV-Water fractions

The interplay between peat and water resulted in limitations in NPV mapping. GV fractions were reliably predicted, a result backed up by Kowalski et al. (2022) and Kowalski et al. (2023) in grasslands (MAE = 7.18% and 6.54%). Tian et al. (2023) similarly predicted GV, NPV, and Soil fractions for different land-cover types (grassland, cropland, forest) using single-date Sentinel-2 RGB indices, validated against UAV-derived fractions. They observed varying performance across GV and NPV fractions, likely due to single-date limitations. However, direct comparison is not feasible, as their validation was conducted at the land-cover type level rather than class-wise. Bare peat fractions were not included in our study, as its occurrence in peatlands is tied to water dynamics rather than vegetation phenology. High water level fluctuation and inundation, which is common in rewetted peatlands (Kreyling et al., 2021; Zerbe et al., 2013; Liu and Lennartz, 2019) was also observed in our study rea. Illustrated well by the permanent Water class (Figure 8); open water bodies dry out in August, revealing bare peat which becomes overgrown by vegetation (Beyer et al., 2021), increasing the fraction of GV until it is again inundated in the next wet season. NPV fractions were less reliably predicted (MAE = 21%) than by Kowalski et al. (2022) and Kowalski et al. (2023) with MAE = 13.7% and 15.38%. Peat, when saturated, resembles water spectrally, while dry peat may resemble NPV, affecting overall NPV prediction accuracies. This highlights the necessity of multi-temporal information and water dynamics in monitoring rewetted peatlands.

Inundation events were most reliably detected in areas of low vegetation. High water fractions for Phragmites, Typha, and Shrubs indicated inundation events in the beginning of the vegetation period, despite comparably dry conditions (Supplementary Figure D). The high water fractions, however, may likely reflect the presence of shadows due to the low canopy density in April and May, revealing shaded areas of water, peat, NPV, GV or a mixture of all. Shadow effects are large in the early and late season, due to the low sun elevation angles (Supplementary Table A). A dense vegetation canopy late in the season can counteract shadow effects, resulting in more reliable water predictions in September compared to April and May. In turn, areas of lower, denser vegetation (e.g., Carex, Figure 12) cast less shadow and therefore yield a more reliable prediction of inundated water area extent throughout the year, as observed for the peak in May. In future studies, the effect of shadow as an additional endmember and its influence on the water class should be tested.

4.3 Class-wise phenology

Differences in Phragmites (*P. australis*) phenology became apparent after combining the species fractions with NPV-GV-Water fractions. The maximum GV fractions indicated different peaks in GV for Phragmites, primarily in August but also as early as June (Figure 11), a pattern which could be observed in field observations (Figure 2, right). This variation might be due to phenotypic plasticity of *P. australis* in response to water table depth and fluctuation (Song et al., 2021; Vretare et al., 2001), which ware possibly caused by the above average precipitation events in July and August 2023. A direct link, however, is difficult to prove given the dominant role of groundwater levels in fen peatlands, and particularly the water level of the adjacent Peene river in this case (Timmermann et al., 2006). The temperature was within average range (Supplementary Figure D), but we cannot account for differences in micro-climate which may result in different phenological expression. Further investigations would be necessary, for example, on detailed groundwater levels, nutrient loads and local temperature.

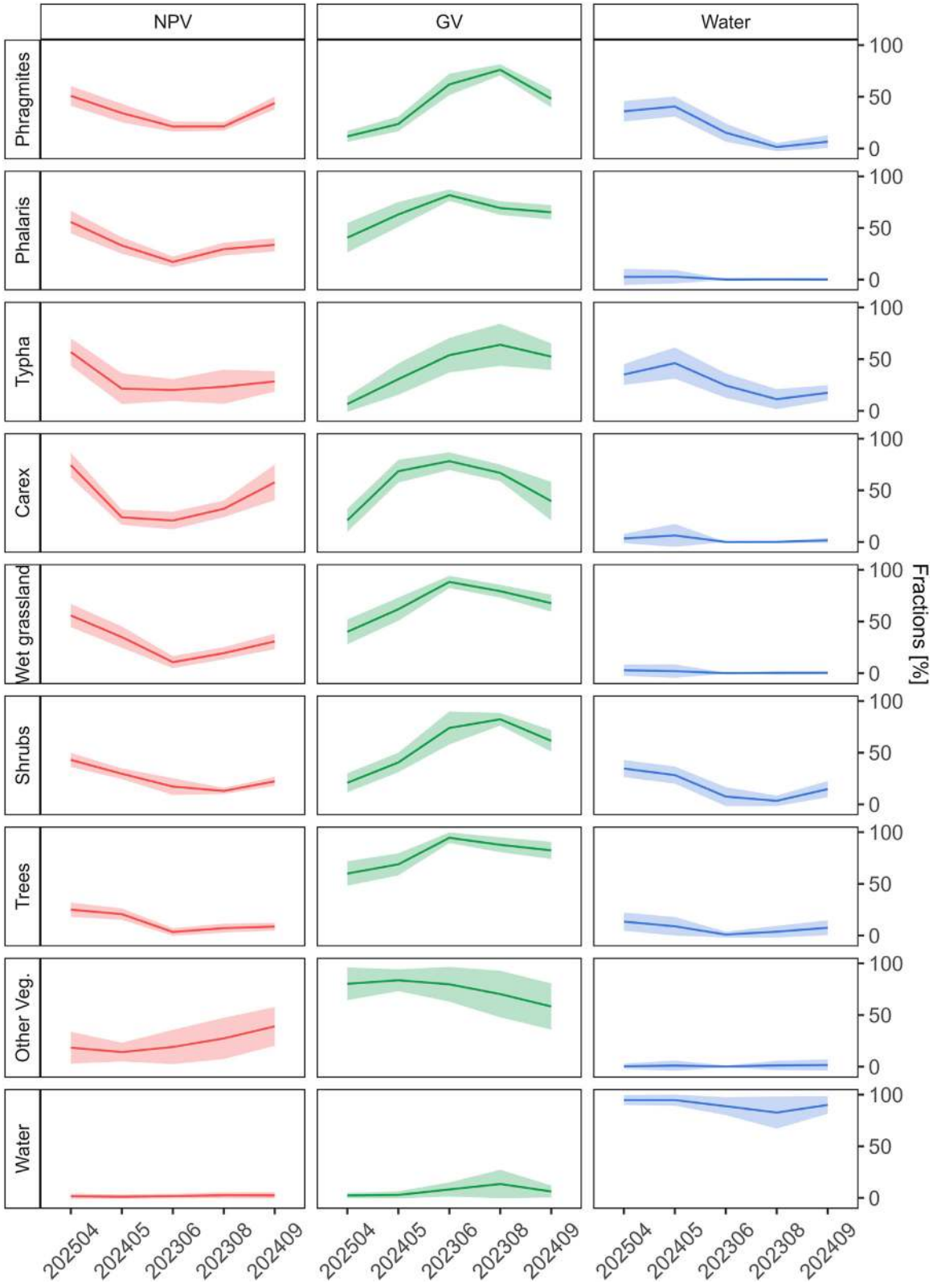


FIGURE 10
Mean NPV, GV and Water fraction ±standard deviation over time for the different classes. Minimum species fraction cover was 70% to ensure high fraction coverage and thus reliable trends. Red = NPV, Green = GV, Blue = Water. Other Veg. = Other Vegetation.

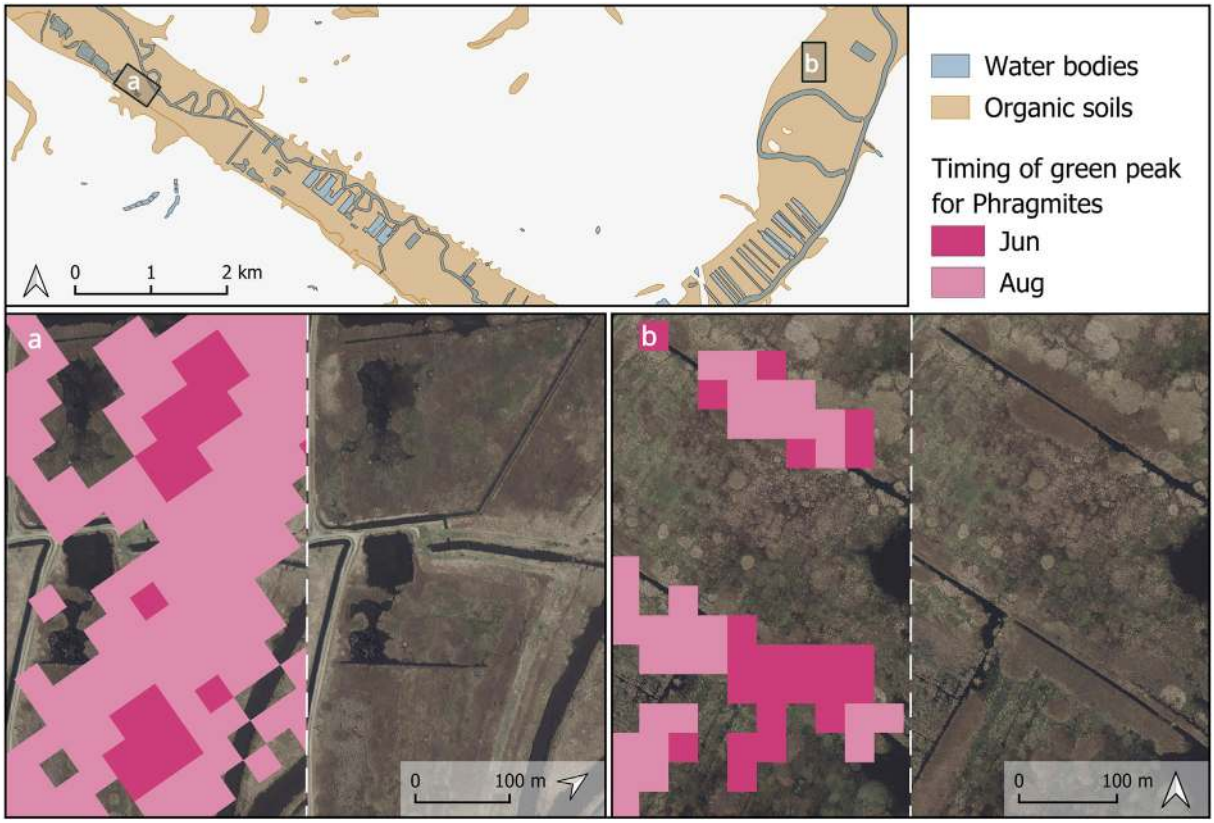


FIGURE 11
Differences in timing of GV peak for Phragmites ≥50%. The location of the subset regions a and b are shown in the top left. Sources: Water bodies were derived from Open Street Map. VHR imagery was acquired on 21 April 2023 and provided by the GeoPortal.MV (https://www.geoportal-mv.de/portal/).



FIGURE 12
Left: *P. australis* NPV early in the season, and GV in summer. Right: *Carex* sp NPV early in the season and GV in summer. *Phragmites* casts more shadow in April, than *Carex*.

If a class comprised different species, such as the Carex class, the separation of different phenological expressions enabled to further split the class on the species levels. The variety in phenology of the different *Carex* species was captured in the endmember data set, e.g., high share in NPV for *C. acuta* but low NPV fractions for *C. acutiformis* and *C. riparia*. With a simple thresholding based on the NPV value in September, the Carex group could be split in *C. riparia* and *C. acutiformis* (low NPV) vs. *C. acuta* (high NPV, Figure 13). However, intra-specific differences in phenology would be neglected with this method, e.g., *C. acuta* with high GV and *C. acutiformis* with high NPV in September.

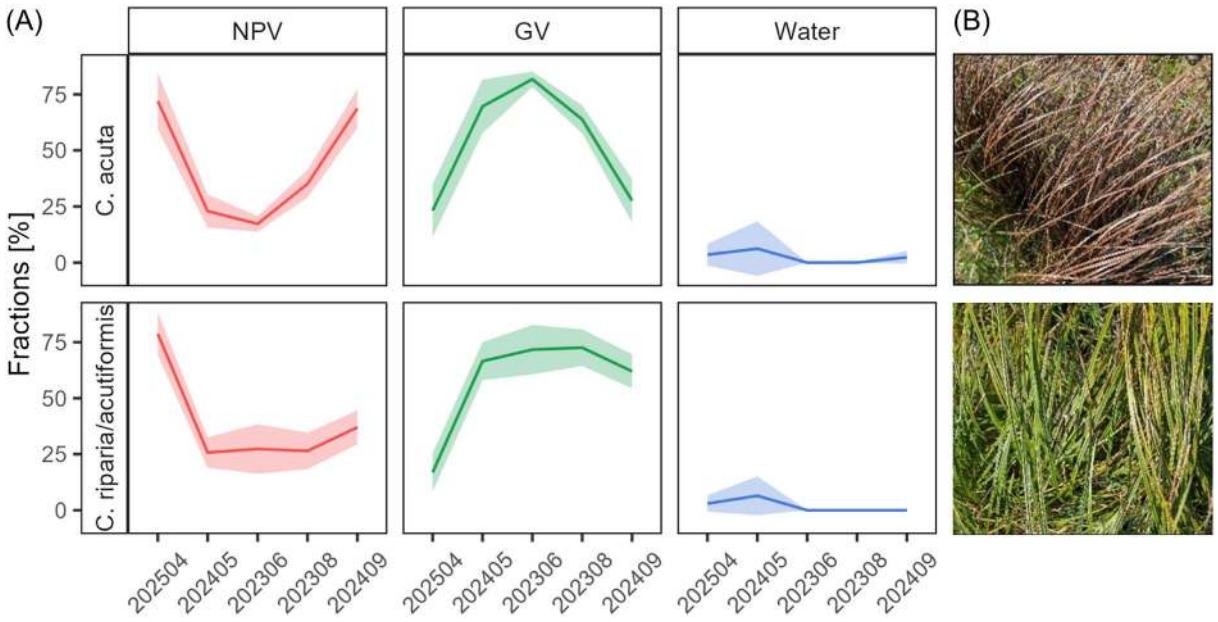


FIGURE 13
(A) Mean NPV, GV and Water fractions ±standard deviation over time for two different phenological trends in the Carex class (Carex > 70%). The different trends were separated based on simple thresholding of NPV values (threshold value = 50% NPV in September 2024). The different phenological trends are representative for *C. acuta* vs. *C. riparia/acutiformis*. **(B)** Top *C. acuta* on 20 September 2024, bottom *C. acutiformis* on 20 September 2024, which is similar to *C. riparia*.

4.4 Methodological considerations

The temporal offset of the validation data to the EnMAP imagery needs to be considered in the validation process. The HyPlant species fractions were based on a single acquisition in 2024, while species fractions from EnMAP were based on multi-temporal imagery from 2023 to 2025. Thus, differences in weather and vegetation phenology over time can reduce prediction accuracies. Further, vegetation patches, e.g., *P. australis* and *Typha* spp., may expand within the 3 years of observation (Packer et al., 2017; Heinz, 2011). These changes on the ground may explain the model error (MAE >15%) to some extent and increase uncertainty of our results. Due to the limited data availability and the fact that we had to join scenes from 3 years to generate a multi seasonal time series, we could not investigate how spatial-temporal changes are represented in results from subsequent years. Such investigation would be worthwhile when a higher data density per years is given. Moreover, the maximum offset between UAV imagery and EnMAP imagery for the NPV-GV-Water validation was 6 days. An offset of 8 days between two UAV acquisitions already showed large differences in NDVI and the extent of inundated water areas (Supplementary Figures E,F). Thus, the offset of a few days between UAV and EnMAP may result in overestimation or underestimation of EnMAP of NPV, GV, and Water fractions. Additionally, the validation with independent classifications from high spatial resolution data is no direct ground truth but provides continuous data for comparably large areas.

Data density plays a key role in monitoring peatlands over time. Here, we used data from three consecutive years, but combined them as if they were from a single vegetation period. For species mapping, the combination may be even better than single year information due to the included seasonal variation (Arasumani et al., 2023; Wolff et al., 2025; Pang et al., 2022). However, regarding phenological variations, wet and dry periods from multiple years may become intermixed (Wolff et al., 2025), so observed trends may not be absolute and cannot be generalized. Upcoming hyperspectral satellite missions (SBG, CHIME) would further increase the temporal resolution than just EnMAP alone, enabling annual species distribution maps and true single year phenological patterns. Systems with higher temporal information, such as Landsat and Sentinel-2 already offer high temporal resolution but are delivered with the expense of decreased spectral resolution. However, testing the transferability on multispectral systems and larger areas is necessary. Further upcoming superspectral sensors may be promising for global monitoring schemes (Dennison et al., 2023).

5 Conclusion

This research showed the suitability of utilizing multi-temporal imaging spectroscopy data (EnMAP) for mapping dominant peatland vegetation and detecting intra-annual changes in vegetation condition and water dynamics in a rewetted peatland landscape. Observed variations in phenological patterns, particularly differences in peak green-up timings for *Phragmites australis*, suggest the potential for using remote sensing data as a proxy for underlying hydrological

gradients driving peatland vegetation communities. However, limitations remain. The high number of vegetation classes and the inherent spectral similarity of peatland vegetation impacted the accuracy of species fraction predictions. The presence of shadow as well as wet open peat affected NPV and water predictions. Despite these limitations, we represent with this work a significant step toward utilizing spaceborne imaging spectroscopy data for monitoring rewetted peatlands on larger scales. The demonstrated ability to track seasonal changes in vegetation and water dynamics provides a basis for assessing the success of rewetting efforts and understanding the drivers of carbon cycling in these critical ecosystems.

Data availability statement

The raw data supporting the conclusions of this article will be made available by the authors, without undue reservation.

Author contributions

CH: Writing – original draft, Methodology, Conceptualization, Software, Investigation, Formal Analysis, Visualization. CW: Writing – review and editing, Methodology, Software. V-DP: Writing – review and editing, Methodology, Software. MS: Funding acquisition, Supervision, Writing – review and editing. SvdL: Resources, Funding acquisition, Supervision, Conceptualization, Writing – review and editing.

Funding

The author(s) declared that financial support was received for this work and/or its publication. This study was mainly financed by the German Space Agency at DLR with resources from the Federal Ministry of Research, Technology and Space (grant number 50EE2234A). VP was funded by the Interdisciplinary Research Center for the Baltic Sea Region (IFZO) of University of Greifswald within the research project Fragmented Transformations (Federal Ministry of Research, Technology and Space; FKZ 01UC2102), CW was funded by Deutsche Forschungsgemeinschaft (DFG) in the project WETSCAPES2.0 (grant number 531801029).

Acknowledgements

We thank DLR for providing the original EnMAP imagery for this research. The EnMAP data are licensed products of DLR (2022), all rights reserved. We thank the student collaborators Amelie Lucks, Malin Stephan, and Enna Drege for their help in fieldwork and validation data generation and Viet-Duc Nguyen, Bernd Bobertz and Matthias Naumann for acquiring and processing UAV imagery. We thank Ariane Tepaß for fruitful discussions and the two reviewers for their valuable feedback.

Conflict of interest

The author(s) declared that this work was conducted in the absence of any commercial or financial relationships that could be construed as a potential conflict of interest.

Generative AI statement

The author(s) declared that generative AI was not used in the creation of this manuscript.

Any alternative text (alt text) provided alongside figures in this article has been generated by Frontiers with the support of artificial intelligence and reasonable efforts have been made to ensure accuracy, including review by the authors wherever possible. If you identify any issues, please contact us.

Publisher's note

All claims expressed in this article are solely those of the authors and do not necessarily represent those of their affiliated organizations, or those of the publisher, the editors and the reviewers. Any product that may be evaluated in this article, or claim that may be made by its manufacturer, is not guaranteed or endorsed by the publisher.

Supplementary material

The Supplementary Material for this article can be found online at: https://www.frontiersin.org/articles/10.3389/fenvs.2026.1805563/full#supplementary-material

References

Arasumani, M., Thiel, F., Pham, V.-D., Hellmann, C., Kaiser, M., and van der Linden, S. (2023). Advancing peatland vegetation mapping by spaceborne imaging spectroscopy. *Ecol. Indic.* 154, 110665. doi:10.1016/j.ecolind.2023.110665

Bantelmann, P., Wyss, D., Pius, E. T., and Kappas, M. (2024). Spectral imaging of grass species in arid ecosystems of Namibia. *Front. Remote Sens.* 5, 1368551. doi:10.3389/frsen.2024.1368551

Beyer, F., Jansen, F., Jurasinski, G., Koch, M., Schröder, B., and Koebsch, F. (2021). Drought years in peatland rewetting: rapid vegetation succession can maintain the net CO_2 sink function. *Biogeosciences* 18, 917–935. doi:10.5194/bg-18-917-2021

Brown, C. F., Kazmierski, M. R., Pasquarella, V. J., Rucklidge, W. J., Samsikova, M., Zhang, C., et al. (2025). AlphaEarth foundations: an embedding field model for accurate and efficient global mapping from sparse label data. *arXiv*. doi:10.48550/arXiv.2507.22291

Cole, B., McMorrow, J., and Evans, M. (2014). Spectral monitoring of moorland plant phenology to identify a temporal window for hyperspectral remote sensing of peatland. *ISPRS J. Photogrammetry Remote Sens.* 90, 49–58. doi:10.1016/j.isprsjprs.2014.01.010

Cooper, S., Okujeni, A., Jänicke, C., Clark, M., van der Linden, S., and Hostert, P. (2020). Disentangling fractional vegetation cover: regression-based unmixing of simulated spaceborne imaging spectroscopy data. *Remote Sens. Environ.* 246, 111856. doi:10.1016/j.rse.2020.111856

Dąbrowska-Zielińska, K., Budzyńska, M., Kowalik, W., Małek, I., Gatkowska, M., Bartold, M., et al. (2012). Biophysical parameters assessed from microwave and pptical data. *Int. J. Electron. Telecommun.* 58, 99–104. doi:10.2478/v10177-012-0013-7

Dąbrowska-Zielińska, K., Budzyńska, M., Tomaszewska, M., Bartold, M., Gatkowska, M., Małek, I., et al. (2014). Monitoring wetlands ecosystems using ALOS PALSAR (L-Band, HV) supplemented by optical data: a case study of Biebrza Wetlands in northeast Poland. *Remote Sens.* 6, 1605–1633. doi:10.3390/rs6021605

Daughtry, C. S. T., Hunt, E. R., and McMurtrey, J. E. (2004). Assessing crop residue cover using shortwave infrared reflectance. *Remote Sens. Environ.* 90, 126–134. doi:10.1016/j.rse.2003.10.023

Dennison, P. E., Lamb, B. T., Campbell, M. J., Kokaly, R. F., Hively, W. D., Vermote, E., et al. (2023). Modeling global indices for estimating non-photosynthetic vegetation cover. *Remote Sens. Environ.* 295, 1–18. doi:10.1016/j.rse.2023.113715

Deutscher Wetterdienst (2025). *Standort teterow*. (Teterow: Deutscher Wetterdienst). Available online at: https://www.dwd.de/DE/leistungen/cdc/cdc_ueberblick-klimadaten.html?nn=16102 (Accessed September 23, 2025).

Dudley, K. L., Dennison, P. E., Roth, K. L., Roberts, D. A., and Coates, A. R. (2015). A multi-temporal spectral library approach for mapping vegetation species across spatial and temporal phenological gradients. *Remote Sens. Environ.* 167, 121–134. doi:10.1016/j.rse.2015.05.004

Edwards, K. R., Glocker, B., Mastný, J., and Picek, T. (2025). Changing environmental conditions impact the phenotypic plasticity of *Carex acuta* and *Glyceria maxima*, two common wet grassland species. *Front. Plant Science* 16, 1–15. doi:10.3389/fpls.2025.1542907

Elmer, K., Kalacska, M., and Arroyo-Mora, J. P. (2021). Mapping the extent of invasive *Phragmites australis* subsp. *australis* from airborne hyperspectral imagery. *Front. Environ. Sci.* 9, 757871. doi:10.3389/fenvs.2021.757871

Elvidge, C. D. (1990). Visible and near infrared reflectance characteristics of dry plant materials. *Int. J. Remote Sens.* 11, 1775–1795. doi:10.1080/01431169008955129

Erkens, G., van der Meulen, M. J., and Middelkoop, H. (2016). Double trouble: subsidence and CO_2 respiration due to 1,000 years of Dutch coastal peatlands cultivation. *Hydrogeology J.* 24, 551–568. doi:10.1007/s10040-016-1380-4

Feilhauer, H., and Schmidtlein, S. (2011). On variable relations between vegetation patterns and canopy reflectance. *Ecol. Inf.* 6, 83–92. doi:10.1016/j.ecoinf.2010.12.004

Feilhauer, H., Faude, U., and Schmidtlein, S. (2011). Combining Isomap ordination and imaging spectroscopy to map continuous floristic gradients in a heterogeneous landscape. *Remote Sens. Environ.* 115, 2513–2524. doi:10.1016/j.rse.2011.05.011

Feilhauer, H., Thonfeld, F., Faude, U., He, K. S., Rocchini, D., and Schmidtlein, S. (2013). Assessing floristic composition with multispectral sensors—A comparison based on monotemporal and multiseasonal field spectra. *Int. J. Appl. Earth Observation Geoinformation* 21, 218–229. doi:10.1016/j.jag.2012.09.002

Flynn, K. C., Chinmayi, H. K., Baath, G. S., Sapkota, B. R., Delhom, C., and Smith, D. R. (2026). UAV-based estimates of corn LAI using hyperspectral and EnMAP spectral resolutions. *Comput. Electron. Agric.* 244, 1–12. doi:10.1016/j.compag.2026.111469

Franz, D., Koebsch, F., Larmanou, E., Augustin, J., and Sachs, T. (2016). High net CO_2 and CH_4 release at a eutrophic shallow lake on a formerly drained fen. *Biogeosciences* 13, 3051–3070. doi:10.5194/bg-13-3051-2016

Frick, A., Steffenhagen, P., Zerbe, S., Timmermann, T., and Schulz, K. (2011). Monitoring of the vegetation composition in rewetted peatland with iterative decision tree classification of satellite imagery. *Photogramm. Fernerkund. Geoinformation* 2011, 109–122. doi:10.1127/1432-8364/2011/0076

Geurts, J. J. M., and Fritz, C. (2018). *Paludiculture pilots and experiments with focus on cattail and reed in the Netherlands*. Technical report. CINDERELLA project. FACCE-JPI ERA-NET Plus on Climate Smart Agriculture. Nijmegen: Radboud University, Radboud University.

Gray, P. C., Ridge, J. T., Poulin, S. K., Seymour, A. C., Schwantes, A. M., Swenson, J. J., et al. (2018). Integrating drone imagery into high resolution satellite remote sensing assessments of estuarine environments. *Remote Sens.* 10, 1–24. doi:10.3390/rs10081257

Guerschman, J. P., Hill, M. J., Renzullo, L. J., Barrett, D. J., Marks, A. S., and Botha, E. J. (2009). Estimating fractional cover of photosynthetic vegetation, non-photosynthetic vegetation and bare soil in the Australian tropical savanna region upscaling the EO-1 hyperion and MODIS sensors. *Remote Sens. Environ.* 113, 928–945. doi:10.1016/j.rse.2009.01.006

Günther, A., Barthelmes, A., Huth, V., Joosten, H., Jurasinski, G., Koebsch, F., et al. (2020). Prompt rewetting of drained peatlands reduces climate warming despite methane emissions. *Nat. Communications* 11, 1644. doi:10.1038/s41467-020-15499-z

Hahn, J., Köhler, S., Glatzel, S., and Jurasinski, G. (2015). Methane exchange in a coastal fen in the first year after flooding--A systems shift. *PLoS One* 10, e0140657. doi:10.1371/journal.pone.0140657

Harris, A., Charnock, R., and Lucas, R. M. (2015). Hyperspectral remote sensing of peatland floristic gradients. *Remote Sens. Environ.* 162, 99–111. doi:10.1016/j.rse.2015.01.029

Heinz, S. I. (2011). *Population biology of* Typha latifolia *L. and* Typha angustifolia *L.: establishment, growth and reproduction in a constructed wetland*. Dissertation. Munich: Technische Universität München. Available online at: https://mediatum.ub.tum.de/doc/1002251/1002251.pdf.

Hijmans, R. J. (2025). Terra: spatial data analysis. Available online at: https://CRAN.R-project.org/package=terra (Accessed May 5, 2026).

Jensen, A. B., Eller, F., and Sorrell, B. K. (2024). Comparative flooding tolerance of Typha latifolia and Phalaris arundinacea in wetland restoration: insights from photosynthetic CO_2 response curves, photobiology and biomass allocation. *Heliyon* 10, e23657. doi:10.1016/j.heliyon.2023.e23657

Kattenborn, T., Fassnacht, F. E., Pierce, S., Lopatin, J., Grime, J. P., and Schmidtlein, S. (2017). Linking plant strategies and plant traits derived by radiative transfer modelling. *J. Veg. Sci.* 28, 717–727. doi:10.1111/jvs.12525

Koebsch, F., Gottschalk, P., Beyer, F., Wille, C., Jurasinski, G., and Sachs, T. (2020). The impact of occasional drought periods on vegetation spread and greenhouse gas exchange in rewetted fens. *Philos. Trans. R. Soc. Lond. Ser. B, Biol. Sci.* 375, 20190685. doi:10.1098/rstb.2019.0685

Kowalski, K., Okujeni, A., Brell, M., and Hostert, P. (2022). Quantifying drought effects in Central European grasslands through regression-based unmixing of intra-annual Sentinel-2 time series. *Remote Sens. Environ.* 268, 1–20. doi:10.1016/j.rse.2021.112781

Kowalski, K., Okujeni, A., and Hostert, P. (2023). A generalized framework for drought monitoring across Central European grassland gradients with Sentinel-2 time series. *Remote Sens. Environ.* 286, 1–18. doi:10.1016/j.rse.2022.113449

Krankina, O. N., Pflugmacher, D., Friedl, M., Cohen, W. B., Nelson, P., and Baccini, A. (2008). Meeting the challenge of mapping peatlands with remotely sensed data. *Biogeosciences* 5, 1809–1820. doi:10.5194/bg-5-1809-2008

Kreyling, J., Tanneberger, F., Jansen, F., van der Linden, S., Aggenbach, C., Blüml, V., et al. (2021). Rewetting does not return drained fen peatlands to their old selves. *Nat. Commun.* 12, 1–8. doi:10.1038/s41467-021-25619-y

Kuprina, K., Haldan, K., Saenko, S., Gulam, M. S., Kreyling, J., Schnittler, M., et al. (2025). How drought and ploidy level shape gene expression and DNA methylation in *Phragmites australis*. *Plant Cell Rep.* 44, 1–19. doi:10.1007/s00299-025-03585-9

Lawniczak, A. E., Zbierska, J., Choiński, A., and Szczepaniak, W. (2010). Response of emergent macrophytes to hydrological changes in a shallow lake, with special reference to nutrient cycling. *Hydrobiologia* 656, 243–254. doi:10.1007/s10750-010-0436-z

Liu, H., and Lennartz, B. (2019). Hydraulic properties of peat soils along a bulk density gradient—A meta study. *Hydrol. Process.* 33, 101–114. doi:10.1002/hyp.13314

Lobert, F., Schwieder, M., Alsleben, J., Broeg, T., Kowalski, K., Okujeni, A., et al. (2025a). Unveiling year-round cropland cover by soil-specific spectral unmixing of Landsat and Sentinel-2 time series. *Remote Sens. Environ.* 318, 114594. doi:10.1016/j.rse.2024.114594

Lobert, F., Schwieder, M., Hostert, P., Gocht, A., and Erasmi, S. (2025b). Characterizing spatio-temporal patterns of winter cropland cover in Germany based on Landsat and Sentinel-2 time series. *Int. J. Appl. Earth Observ. Geoinformation* 142, 104728. doi:10.1016/j.jag.2025.104728

Lopatin, J., Dolos, K., Hernández, H. J., Galleguillos, M., and Fassnacht, F. E. (2016). Comparing generalized linear models and random forest to model vascular plant species richness using LiDAR data in a natural forest in central Chile. *Remote Sens. Environ.* 173, 200–210. doi:10.1016/j.rse.2015.11.029

Mandl, L., Viana-Soto, A., Seidl, R., Stritih, A., and Senf, C. (2024). Unmixing-based forest recovery indicators for predicting long-term recovery success. *Remote Sens. Environ.* 308, 1–13. doi:10.1016/j.rse.2024.114194

McPartland, M. Y., Kane, E. S., Falkowski, M. J., Kolka, R., Turetsky, M. R., Palik, B., et al. (2018). The response of boreal peatland community composition and NDVI to hydrologic change, warming, and elevated carbon dioxide. *Glob. Change Biol.* 25, 93–107. doi:10.1111/gcb.14465

McPartland, M. Y., Falkowski, M. J., Reinhardt, J. R., Kane, E. S., Kolka, R., Turetsky, M. R., et al. (2019). Characterizing boreal peatland plant composition and species diversity with hyperspectral remote sensing. *Remote Sens.* 11, 1685. doi:10.3390/rs11141685

Middleton, M., Närhi, P., Arkimaa, H., Hyvönen, E., Kuosmanen, V., Treitz, P., et al. (2012). Ordination and hyperspectral remote sensing approach to classify peatland biotopes along soil moisture and fertility gradients. *Remote Sens. Environ.* 124, 596–609. doi:10.1016/j.rse.2012.06.010

Minasny, B., Adetsu, D. V., Aitkenhead, M., Artz, R. R. E., Baggaley, N., Barthelmes, A., et al. (2023). Mapping and monitoring peatland conditions from global to field scale. *Biogeochemistry* 167, 383–425. doi:10.1007/s10533-023-01084-1

Mrotzek, A., Michaelis, D., Günther, A., Wrage-Mönnig, N., and Couwenberg, J. (2020). Mass balances of a drained and a rewetted peatland: on former losses and recent gains. *Soil Syst.* 4 (16), 1–14. doi:10.3390/soilsystems4010016

Nagler, P. L., Daughtry, C. S. T., and Goward, S. N. (2000). Plant litter and soil reflectance. *Remote Sens. Environ.* 71, 207–215. doi:10.1016/s0034-4257(99)00082-6

Nagler, P. L., Inoue, Y., Glenn, E. P., Russ, A. L., and Daughtry, C. S. T. (2003). Cellulose absorption index (CAI) to quantify mixed soil–plant litter scenes. *Remote Sens. Environ.* 87, 310–325. doi:10.1016/j.rse.2003.06.001

Nill, L., Grünberg, I., Ullmann, T., Gessner, M., Boike, J., and Hostert, P. (2022). Arctic shrub expansion revealed by Landsat-derived multitemporal vegetation cover fractions in the Western Canadian Arctic. *Remote Sens. Environ.* 281, 113228. doi:10.1016/j.rse.2022.113228

Okujeni, A., van der Linden, S., Tits, L., Somers, B., and Hostert, P. (2013). Support vector regression and synthetically mixed training data for quantifying urban land cover. *Remote Sens. Environ.* 137, 184–197. doi:10.1016/j.rse.2013.06.007

Okujeni, A., van der Linden, S., Suess, S., and Hostert, P. (2017). Ensemble learning from synthetically mixed training data for quantifying urban land cover with support vector regression. *IEEE J. Sel. Top. Appl. Earth Observ. Remote Sens.* 10, 1640–1650. doi:10.1109/JSTARS.2016.2634859

Okujeni, A., Canters, F., Cooper, S. D., Degerickx, J., Heiden, U., Hostert, P., et al. (2018). Generalizing machine learning regression models using multi-site spectral libraries for mapping vegetation-impervious-soil fractions across multiple cities. *Remote Sens. Environ.* 216, 482–496. doi:10.1016/j.rse.2018.07.011

Oppelt, N. (2002). Monitoring of plant chlorophyll and nitrogen status using the airborne imaging spectrometer AVIS. Dissertation. Munich: Fakultät der Geowissenschaften.

Packer, J. G., Meyerson, L. A., Skálová, H., Pyšek, P., and Kueffer, C. (2017). Biological Flora of the British isles: phragmites australis. *J. Ecol.* 105, 1123–1162. doi:10.1111/1365-2745.12797

Pang, Y., Räsänen, A., Lindholm, V., Aurela, M., and Virtanen, T. (2022). Detecting peatland vegetation patterns with multi-temporal field spectroscopy. *GIScience Remote Sens.* 59, 2111–2126. doi:10.1080/15481603.2022.2152303

Pflugmacher, D., Krankina, O. N., and Cohen, W. B. (2007). Satellite-based peatland mapping: potential of the MODIS sensor. *Glob. Planet. Change* 56, 248–257. doi:10.1016/j.gloplacha.2006.07.019

Pham, V.-D., Thiel, F., Frantz, D., Okujeni, A., Schug, F., and van der Linden, S. (2024). Learning the variations in annual spectral-temporal metrics to enhance the transferability of regression models for land cover fraction monitoring. *Remote Sens. Environ.* 308, 114206. doi:10.1016/j.rse.2024.114206

Priem, F., Okujeni, A., van der Linden, S., and Canters, F. (2019). Comparing map-based and library-based training approaches for urban land-cover fraction mapping from Sentinel-2 imagery. *Int. J. Appl. Earth Observ. Geoinformation* 78, 295–305. doi:10.1016/j.jag.2019.02.003

Rascher, U., Alonso, L., Burkart, A., Cilia, C., Cogliati, S., Colombo, R., et al. (2015). Sun-induced fluorescence - a new probe of photosynthesis: first maps from the imaging spectrometer HyPlant. *Global change biology*21, 4673–4684. doi:10.1111/gcb.13017

R Core Team (2022). *R: a language and environment for statistical computing*. Vienna, Austria. Available online at: https://www.R-project.org/.

Räsänen, A., and Virtanen, T. (2019). Data and resolution requirements in mapping vegetation in spatially heterogeneous landscapes. *Remote Sens. Environ.* 230, 111207. doi:10.1016/j.rse.2019.05.026

Reddig, F., Hütt, C., Jenal, A., Wolf, J., and Bareth, G. (2025). The invisible plant: estimating fractional vegetation cover of *Tillandsia landbeckii* in the Atacama Desert using hyperspectral EnMAP and high-resolution validation data. *Photogramm. Fernerkund. Geoinformation* 93, 583–609. doi:10.1007/s41064-025-00358-7

Salko, S.-S., Hovi, A., Burdun, I., Juola, J., and Rautiainen, M. (2024). Hyperspectral characterization of vegetation in hemiboreal, boreal and Arctic peatlands using a geographically extensive field dataset. *Ecol. Inf.* 82, 102772. doi:10.1016/j.ecoinf.2024.102772

Salko, S.-S., Hovi, A., Burdun, I., Juola, J., Karlqvist, S., and Rautiainen, M. (2025). Assessing species fractional cover and α-Diversity in boreal peatlands accross trophic levels using hyperspectral data. *Ecol. Evolution* 15, e71941. doi:10.1002/ece3.71941

Scheffler, D., Hollstein, A., Diedrich, H., Segl, K., and Hostert, P. (2017). AROSICS: an automated and robust open-source image co-registration software for multi-sensor satellite data. *Remote Sens.* 9, 676. doi:10.3390/rs9070676

Schug, F., Frantz, D., Okujeni, A., van der Linden, S., and Hostert, P. (2020). Mapping urban-rural gradients of settlements and vegetation at national scale using Sentinel-2 spectral-temporal metrics and regression-based unmixing with synthetic training data. *Remote Sens. Environ.* 246, 111810. doi:10.1016/j.rse.2020.111810

Schulz, K., Timmermann, T., Steffenhagen, P., Zerbe, S., and Succow, M. (2011). The effect of flooding on carbon and nutrient standing stocks of helophyte biomass in rewetted fens. *Hydrobiologia* 674, 25–40. doi:10.1007/s10750-011-0782-5

Siegmann, B., Alonso, L., Celesti, M., Cogliati, S., Colombo, R., Damm, A., et al. (2019). The high-performance airborne imaging spectrometer HyPlant—from raw images to top-of-canopy reflectance and fluorescence products: introduction of an automatized processing chain. *Remote Sens.* 11, 2760. doi:10.3390/rs11232760

Song, H., Guo, X., Yu, X., Liu, L., Wang, N., Eller, F., et al. (2021). Is there evidence of local adaptation of *Phragmites australis* to water level gradients and fluctuation frequencies? *Sci. Total Environ.* 756, 144065. doi:10.1016/j.scitotenv.2020.144065

Specht, D. F. (1991). A general regression neural network. *IEEE Trans. Neural Networks* 2, 568–576. doi:10.1109/72.97934

Stanimirova, R., Graesser, J., Olofsson, P., and Friedl, M. A. (2022). Widespread changes in 21st century vegetation cover in Argentina, Paraguay, and Uruguay. *Remote Sens. Environ.* 282, 113277. doi:10.1016/j.rse.2022.113277

Steenvoorden, J., and Limpens, J. (2023). Upscaling peatland mapping with drone-derived imagery: impact of spatial resolution and vegetation characteristics. *GIScience Remote Sens.* 60, 2267851. doi:10.1080/15481603.2023.2267851

Storch, T., Honold, H.-P., Chabrillat, S., Habermeyer, M., Tucker, P., Brell, M., et al. (2023). The EnMAP imaging spectroscopy mission towards operations. *Remote Sens. Environ.* 294, 113632. doi:10.1016/j.rse.2023.113632

Succow, M., and Jeschke, L. (1986). *Moore in der Landschaft*. Leipzig: Urania-Verlag, p. 285.

Suess, S., van der Linden, S., Okujeni, A., Griffiths, P., Leitão, P. J., Schwieder, M., et al. (2018). Characterizing 32 years of shrub cover dynamics in southern Portugal using annual Landsat composites and machine learning regression modeling. *Remote Sens. Environ.* 219, 353–364. doi:10.1016/j.rse.2018.10.004

Tanneberger, F., Tegetmeyer, C., Dylawerski, M., Flade, M., and Joosten, H. (2009). Commercially cut reed as a new and sustainable habitat for the globally threatened Aquatic Warbler. *Biodivers. Conservation* 18, 1475–1489. doi:10.1007/s10531-008-9495-0

Tian, J., Zhang, Z., Philpot, W. D., Tian, Q., Zhan, W., Xi, Y., et al. (2023). Simultaneous estimation of fractional cover of photosynthetic and non-photosynthetic vegetation using visible-near infrared satellite imagery. *Remote Sens. Environ.* 290, 113549. doi:10.1016/j.rse.2023.113549

Tiemeyer, B., Albiac Borraz, E., Augustin, J., Bechtold, M., Beetz, S., Beyer, C., et al. (2016). High emissions of greenhouse gases from grasslands on peat and other organic soils. *Glob. Change Biol.* 22, 4134–4149. doi:10.1111/gcb.13303

Timmermann, T., Margóczi, K., Takács, G., and Vegelin, K. (2006). Restoration of peat-forming vegetation by rewetting species-poor fen grasslands. *Appl. Veg. Sci.* 9, 241–250. doi:10.1111/j.1654-109X.2006.tb00673.x

UBA (Umweltbundesamt) (2022). Submission under the United Nations Framework Convention on Climate change and the Kyoto protocol 2022. National inventory report for the German greenhouse gas inventory 1990–2020. *Clim. Change*, 25. Available online at: https://www.umweltbundesamt.de/publikationen/berichterstattung-unter-der-klimarahmenkonvention-7 (Accessed December 17, 2025).

Uellendahl, K., Hirschelmann, S., and Abel, S. (2023). Treibhausgas-Emissionen der moorreichen Bundesländer und die Rolle der organischen Böden. Greifswald Mire Centre. Available online at: https://www.greifswaldmoor.de/informationspapiere.html (Accessed January 14, 2026).

UNEP (2022). "Global Peatlands Assessment: the State of the World's Peatlands. Evidence for action toward the conservation, restoration, and sustainable management of peatlands," in *Main report*. Nairobi: United Nations Environment Programme.

Verrelst, J., Halabuk, A., Atzberger, C., Hank, T., Steinhauser, S., and Berger, K. (2023). A comprehensive survey on quantifying non-photosynthetic vegetation cover and biomass from imaging spectroscopy. *Ecol. Indic.* 155, 110911. doi:10.1016/j.ecolind.2023.110911

Vretare, V., Weisner, S. E. B., Strand, J. A., and Granéli, W. (2001). Phenotypic plasticity in *Phragmites australis* as a functional response to water depth. *Aquat. Bot.* 69, 127–145. doi:10.1016/s0304-3770(01)00134-6

Vroom, R. J. E., Xie, F., Geurts, J. J. M., Chojnowska, A., Smolders, A. J. P., Lamers, L. P. M., et al. (2018). *Typha latifolia* paludiculture effectively improves water quality and reduces greenhouse gas emissions in rewetted peatlands. *Ecol. Eng.* 124, 88–98. doi:10.1016/j.ecoleng.2018.09.008

Waard, F., Connolly, J., Barthelmes, A., Joosten, H., and van der Linden, S. (2024). Remote sensing of peatland degradation in temperate and boreal climate zones – a review of the potentials, gaps, and challenges. *Ecol. Indic.* 166, 112437. doi:10.1016/j.ecolind.2024.112437

Wittnebel, M., Frank, S., and Tiemeyer, B. (2023). *[Datensatz] Aktualisierte Kulisse organischer Böden in Deutschland*. [Dataset] Updated map of organic soils in Germany (English).

Wolff, F., Kolari, T. H. M., Räsänen, A., Tahvanainen, T., Korpelainen, P., Villoslada, M., et al. (2025). Interannual spectral consistency and spatial uncertainties in UAV -based detection of boreal and subarctic mire plant communities. *Remote Sens. Ecol. Conservation* 11, 719–739. doi:10.1002/rse2.70017

Wright, N., Duncan, J. M. A., Callow, J. N., Thompson, S. E., and George, R. J. (2025). Training sensor-agnostic deep learning models for remote sensing: achieving state-of-the-art cloud and cloud shadow identification with OmniCloudMask. *Remote Sens. Environ.* 322, 114694. doi:10.1016/j.rse.2025.114694

Yilmaz, V., Serifoglu Yilmaz, C., Belgiu, M., Candiani, G., Pepe, M., Boschetti, M., et al. (2026). Fusion of EnMAP/PRISMA hyperspectral and Sentinel-2 multispectral imagery for estimating crop traits. *Int. J. Remote Sens.* 47, 1699–1726. doi:10.1080/01431161.2026.2612849

Zak, D., Wagner, C., Payer, B., Augustin, J., and Gelbrecht, J. (2010). Phosphorus mobilization in rewetted fens: the effect of altered peat properties and implications for their restoration. *Ecol. Appl.* 20, 1336–1349. doi:10.1890/08-2053.1

Zerbe, S., Steffenhagen, P., Parakenings, K., Timmermann, T., Frick, A., Gelbrecht, J., et al. (2013). Ecosystem service restoration after 10 years of rewetting peatlands in NE Germany. *Environ. Manage.* 51, 1194–1209. doi:10.1007/s00267-013-0048-2